Chapter 1

Introduction

1-1 An Overview of Cu Damascene Integration Process Flow

As the ultra-large semiconductor integration (ULSI) line width decreases, RC delay becomes a more serious problem (shown in Figure1-1). Equaction 1-1 is the RC delay time realte equation.

$$RC = 2\rho\varepsilon_o\varepsilon(4L^2/P^2 + L^2/T^2) \quad (1\text{-}1)$$

ρ: Resistivity of metal line.

ε: Dielectric constant of metal line.

ε_o: Dielectric constant of Air.

L: Length of metal line.

P: Pitch of metal line.

T: Thickness of metal line.

The replacement of aluminum by copper (Cu) has been proposed for line widths (P) smaller than 0.13 μm because copper reduces resistivity (ρ) (from Table 1-1) and will reduce RC delay (from Equaction 1-1). Besides, Cu will also improve electro-migration (EM) (from Table 1-1).[1] Figure 1-2 shows the complete Cu damascene integration process flow. The process steps are low K dielectric constant material etching, Cu diffusion barrier layer deposition, Cu seed layer deposition, Cu film deposition, Cu chemical mechanical polish (CMP) removes main Cu film, top Cu diffusion barrier removes, post Cu CMP cleaning and Cu capping layer cap. I will explain step by step as follows.

1-1.1 Low K Dielectric Constant Material Etching

This step uses photolithography method to transfer mask patterns to photoresisivity, and then uses etching method to pattern the low K dielectric constant material.

1-1.2 Cu Diffusion Barrier Deposition

Unfortunately, Cu readily diffuses into Si and, therefore, it influences device performance; for example, the introduction of Cu into Si transistors leads to deep-level doping that influences the minor carrier lifetime and increases the junction leakage current.[2] Preventing Cu from diffusing requires that the diffusion barrier between Si and Cu be increased. The question then arises: What kind of diffusion barrier is most useful? Several researchers have demonstrated that TaN_X provides good performance: it has a relatively high melting temperature and it is thermodynamically stable with respect to Cu (shown in Figure 1-3). Reactive sputtering physical vapor deposition (PVD) TaN_X as Cu diffusion barrier thin film is using below 0.13 μm Cu process. Figure 1-4 shows some sputtering PVD technologies. The trends are from normal sputtering, collimated sputtering; long throw sputtering to ionized sputtering. Some metal organic chemical vapor deposition (MOCVD) Cu diffusion barrier layers are developed on below 45nm Cu process.

1-1.3 Cu Seed Layer Deposition

The Cu film is deposited by using electro chemical plating (ECP) method and the ECP process needs a Cu seed layer to conduct electro current to form the Cu film. Sputtering PVD Cu seed layer is using below 0.13 μm Cu process. MOCVD Cu seed layer is developed on below 45nm Cu process. Figure 1-5 shows MOCVD Cu

precursor: (Hfac)Cu(TMVS) (CupraSelect^{TM}) and reaction equaton.

1-1.4 Cu Film Deposition

Using Cu ECP method to deposite Cu film has some advantages: low cost (no vacuum required), room temperature deposition and high deposition rate. But has some disadvantages: gap filling challenge, impurity control and additive consumed. Figure 1-6 shows Cu ECP mechanism and Cu ECP solution contents. The accelerator, suppressor and level three additives chemical properities have big influence for Cu ECP technology especially on below 45nm Cu process.

1-1.5 Cu CMP Process

Cu was proven not to be easily etched by plasma. As the Cu CMP process is been developed (shown in Figure 1-7), the Cu damascene process has been made practical.[3] Unfortunately, the properties of copper are such that CMP has produced many defects, including microscratching, dishing, erosion and reduced yield (shown in Figure 1-8).[4] Equation 1-2 is Preston equation.

$$RR = H / T = K\ p * P * S / T \qquad (1\text{-}2)$$

RR: Remove rate.

H: Change in height of surface.

T: Elapsed time.

Kp: Preston coefficient.

P: Down pressure.

S/T: Linear velocity of the pad relative to the work piece.

Cu CMP process is using below 0.13 μm Cu process. Cu electron polish (EP) is developed on below 45nm Cu process. Figure 1-9 shows Cu EP mechanism. EP has

some advantages: stress free (good for fragile low-k materials), no scratch and no particle on copper surfaces. But has some disadvantages: find suitable protect additives and End-point detection.

1-1.6 Cu CMP Post Clean

After Cu CMP the Cu surface residues some contaminations including abrasive parricales of Cu CMP slurry, BTAs of Cu CMP slurry, Surfactants of Cu CMP slurry and other organic/inorganic contaminations. So we need clean out the contaminations.

1-1.7 Cu Film Capping Layer

When the Cu process reaches below 45nm the current density will become huge. It will induce a big EM effect. So we need cap a suitable material on Cu film by selective electroless deposition on Cu film surface. Figure 1-10 shows Cu film capping layer process.

1-2 An Overview of Microfluidic Biochip

Biochips have potential applications in the fundamental research in life sciences, the development of new drugs, clinical disease diagnosis, food security and the chemical industry, among other areas.[5-12] Among commercialized biochips, DNA chips that contain thousands of microscopic DNA probes per unit area have been well developed and effective. They can be used to analyze the expression of multiple genes simultaneously. Conventional analysis of gene expression uses many instruments for the preparation, amplification and final detection of sample. However, biotechnical micro electro mechanical systems (BioMEMS) replace large biochemical instruments with a small LOC which facilitates a complete set of successive biochemical

experiment steps on a microchip and integrates multiply functions automated laboratory.[13] LOC is fully/highly automated, lightweight, easy to use, low cost, short test cycle time and reduce the need for samples.

1-2.1 Sample Preparation

The complexity of blood samples (shown in Figure 1-11) requires tedious procedures to extract, separate, condense and amplify the desired DNA. Several methods of biochemical sample-preparation are currently available, only well-trained biochemists can perform these complicated DNA extraction procedures. Auxiliary biochemical reagents or apparatus have been developed for general operators, however, these reagents and apparatus are expensive and the procedures are still complicated. The traditional bead method of DNA extraction is also complicated and time-consuming. Using DNA extraction beads fixing on microfluidic channels to accelerate the preparation of the sample and to overcome the aforementioned difficulties has developed a sample-preparation chip. Fixing DNA extraction beads on the chip reduces the amount of sample required, simplifying and fully automating the procedure.

1-2.2 Sample Amplify

We use polymerase chain reaction (PCR) to ampilify the specific region of DNA. Kary Mullis developed PCR at mid-1980s. Using PCR can maxium ampilifyc10^5 specific region of DNA. Figure 1-12 shows the PCR ampilify processes including deneature, annealing and extension. Figure 1-13 shows PCR amplify mechanism. By the end of n cycles: 2^{n-2} amplicons (double-stranded DNA).

1-2.3 Detection

The complementary strand DNA can act hybridization and not complementary strand DNA can’t act hybridization (shown in Figure1-14). Using this mechanism we can detection the DNA sample that are complementary strand DNA. We can label Florence group on the design DNA target. If DNA can hybridize to form complementary strand DNA then we can see the Florence.

References

[1] C. Y. Chang and S. M. Sze, ULSI Technology, McGraw-Hill, New York (1996) 371.

[2] Y. Shacham`-Diamand, J. Li, J. O. Olowlafe, S.,Russel, Y.,Tamou and J.W. Mayer, Proc 9 Bienn Univ. Gov. Ind. Microelectron Symp. Publ by IEEE Service Center, Piscataway, NJ (IEEE cat. n 91ch3027-0) 210.

[3] K. H. Holland and etal , "Achieving CMP Manufacturability in the Current Aluminum and Future Copper Damascene Interconnection Technologies", Semiconductor Fabtech-8th edition (1998) 217.

[4] Stocckl, P.; Saville, B.; Kavanagh, J.; Dellwig, T. "Advanced cu CMP defect excursion control for leading edge micro-processor manufacturing" Advanced Semiconductor Manufacturing IEEE/SEMI Conference and Workshop (2002) 92 -97.

[5] Francia, Girolamo Di, Ferrara, Vera La, Manzo, Sonia, Chiavarini, Salvatore, Towards a label-free optical porous silicon DNA sensor. Biosensors and Bioelectronics, 21(2005) 661-665.

[6] Liu, Wen-Tso, Zhu, Liang, Environmental microbiology-on-a-chip and its future impacts. Trends in Biotechnology, 23 (2005) 174-179.

[7] Wang, Chih-Hao, Lee, Gwo-Bin, Automatic bio-sampling chips integrated with micro-pumps and micro-valves for disease detection. Biosensors and Bioelectronics, 21 (2005) 419-425.

[8] Di Francia, G., Castaldo, A., Massera, E., Nasti, I., Quercia, L., Rea, I., A very sensitive porous silicon based humidity sensor. Sensors & Actuators: B. 111 (2005) 135-139.

[9] Campàs, M., Katakis, I., DNA biochip arraying, detection and amplification

strategies. Trends in Analytical Chemistry, 23 (2004) 49-62.

[10] Cheng, Yi-Ting, Pun, Ching-Chin, Tsai, Chien-Ying, Chen, Ping-Hei, An array-based CMOS biochip for electrical detection of DNA with multilayer self-assembly gold nanoparticles. Sensors & Actuators: B. 109 (2005) 249-255.

[11] Antje J. Baeumner, Richard N. Cohen, Vonya Miksic, Junhong Min, RNA biosensor for the rapid detection of viable Escherichia coli in drinking water. Biosensors and Bioelectronics, 18 (2003) 405-413.

[12] Wenting Zhao, Shanjing Yao, I.-Ming Hsing, A microsystem compatible strategy for viable *Escherichia coli* detection. Biosensors and Bioelectronics, 21 (2006) 1163-1170.

[13] Masaki Yamaguchi, Shigenori Kambe, Takashi Eto, Masaru Yamakoshi, Takuji Kouzuma, Nobuyuki Suzuki, Biosensors and Bioelectronics, 21 (2005) 426-432.

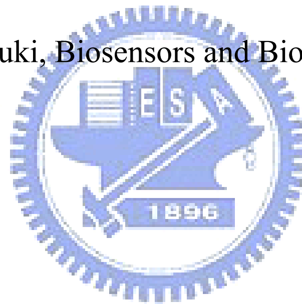

Table 1-1: Ag, Cu, Au and Al metals properties table.

Metal	Ag	Cu	Au	Al
ρ (μΩ-cm)	1.59	1.67	2.35	2.66
	962	1085	1064	660
Thermal conductivity ($Wcm^{-1}K^{-1}$)	4.25	3.98	3.15	2.38
Temperature coefficient of resivity ($^{o}C^{-1}$)	0.0041	0.0043	0.004	0.0045
Thermal expansion coefficient ($10^{-6}K^{-1}$)	19.1	17	14.2	23.5
EM Endurance (Compare to Al)	10	20	20	1

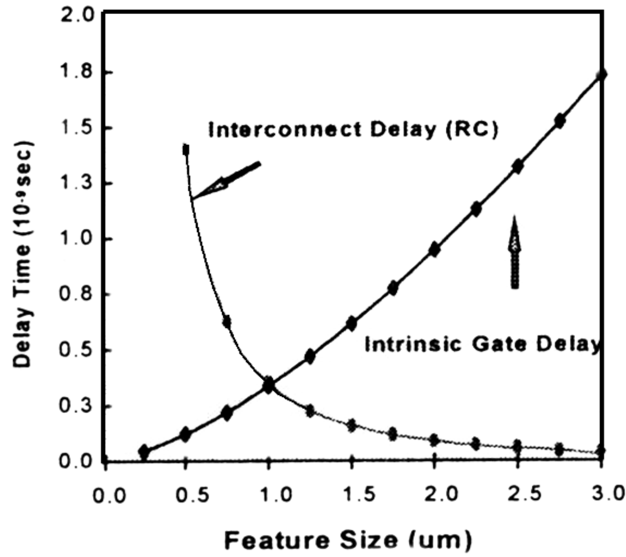

Figure 1-1: The relationship of device gate length and inter connect metal line pitch with RC delay time.

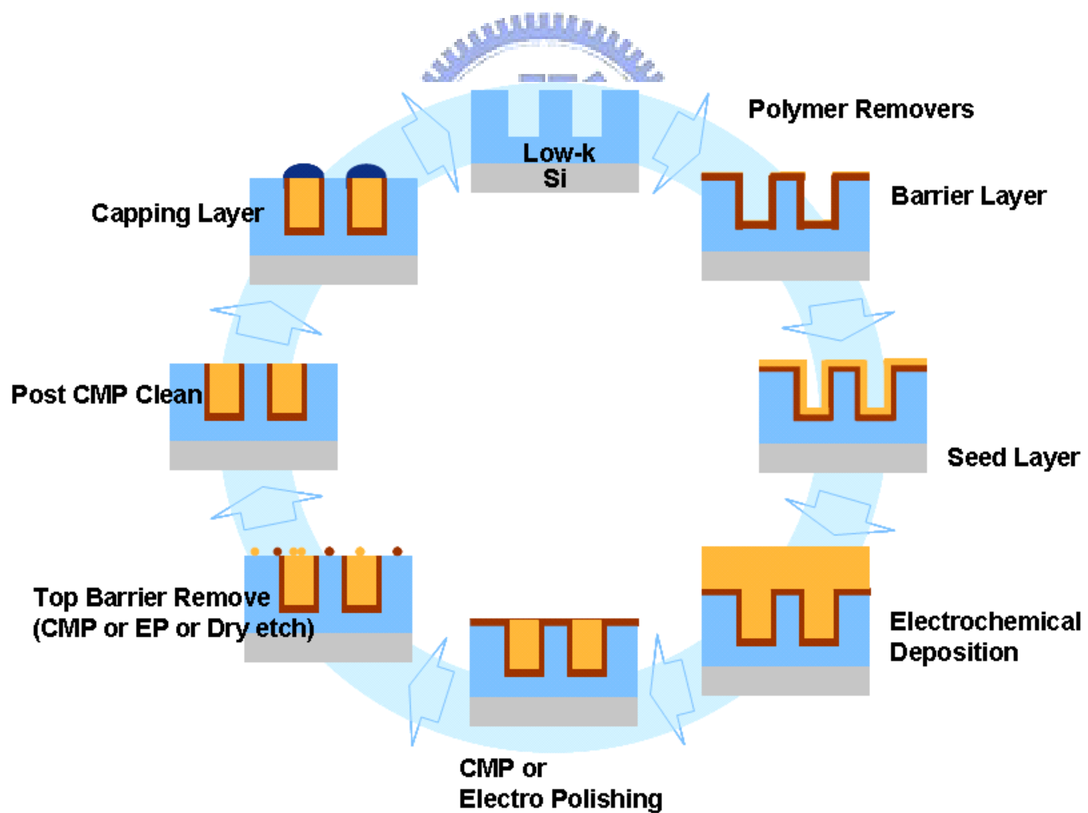

Figure 1-2: Complete Cu damascene integration process flow.

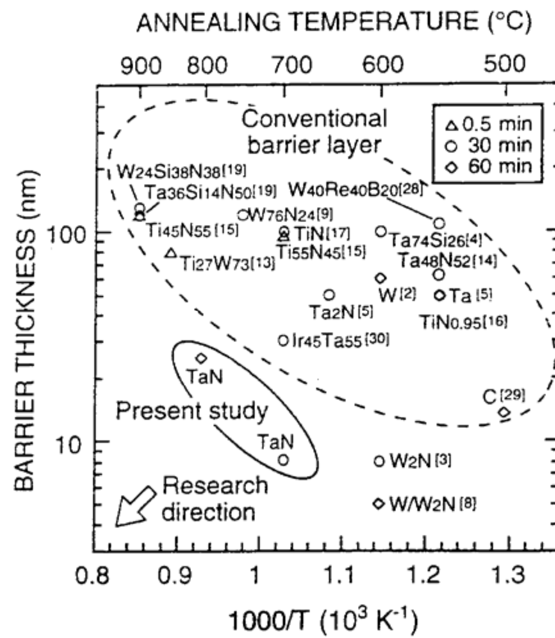

Figure 1-3. The relationship between diffusion barrier thickness and thermal stability.

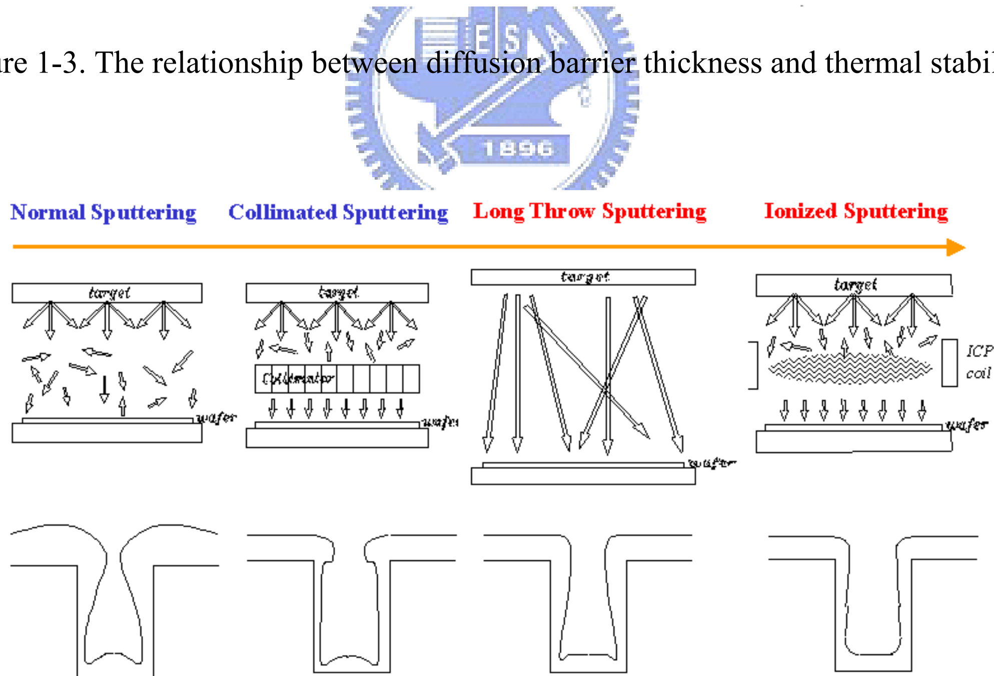

Figure 1-4: Sputtering PVD technologies.

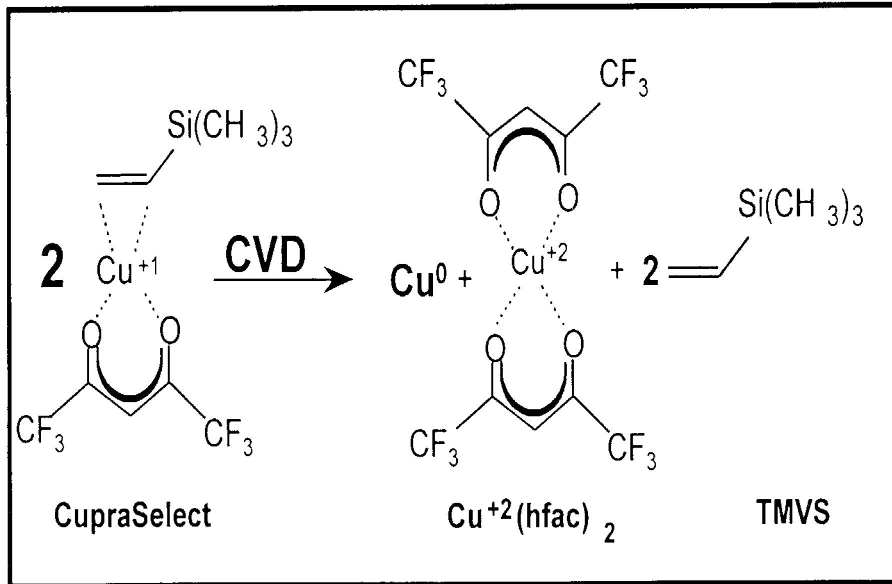

Figure 1-5: MOCVD Cu precursor: (Hfac)Cu(TMVS) (CupraSelect^{TM}) and reaction equation.

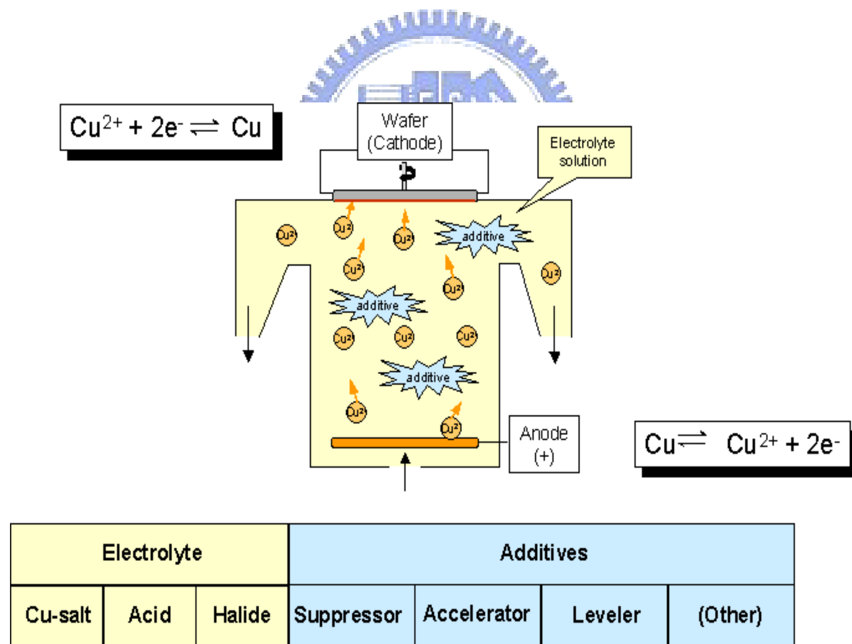

Electrolyte			Additives			
Cu-salt	Acid	Halide	Suppressor	Accelerator	Leveler	(Other)

Figure 1-6: Cu ECP mechanism and Cu ECP solution contents.

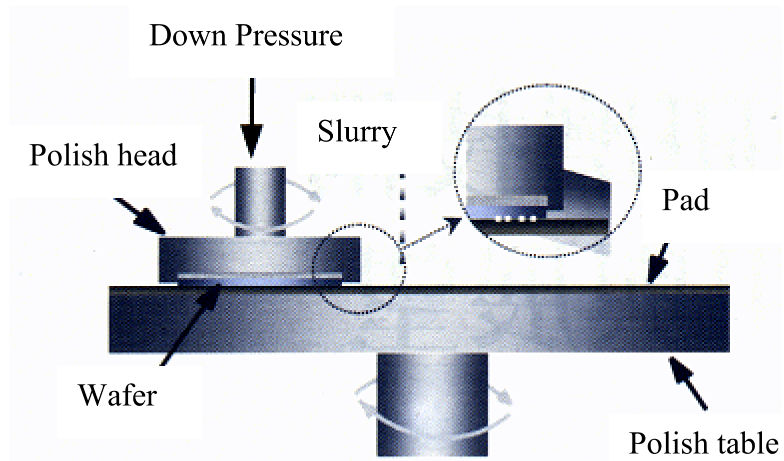

Figure 1-7: CMP process illustration.

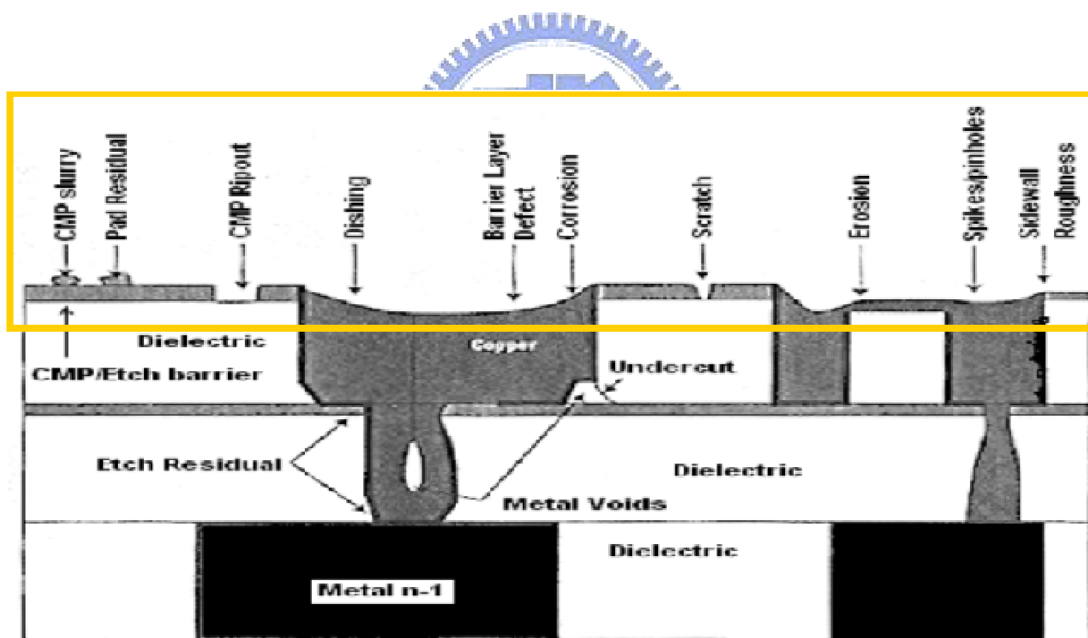

Figure 1-8: Cu CMP process defects.

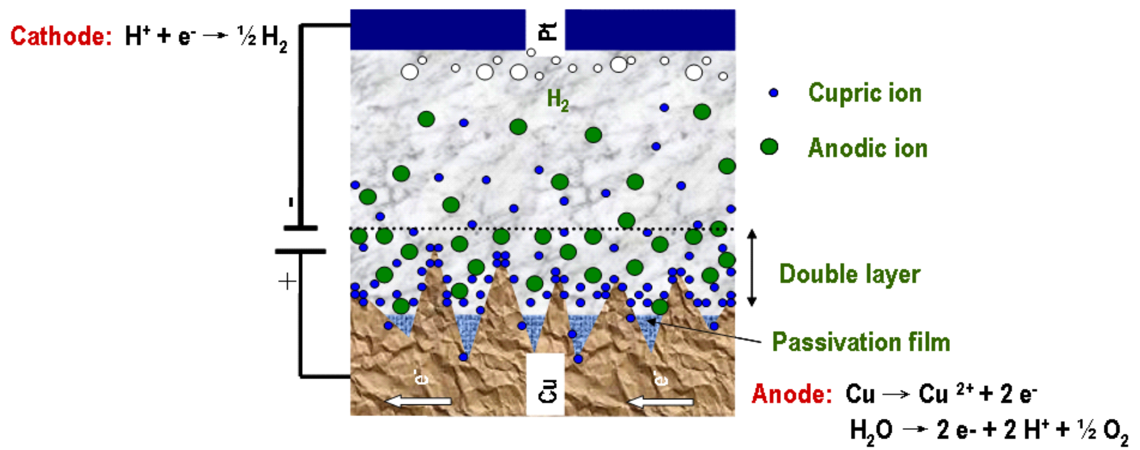

Figure 1-9: Cu EP mechanism.

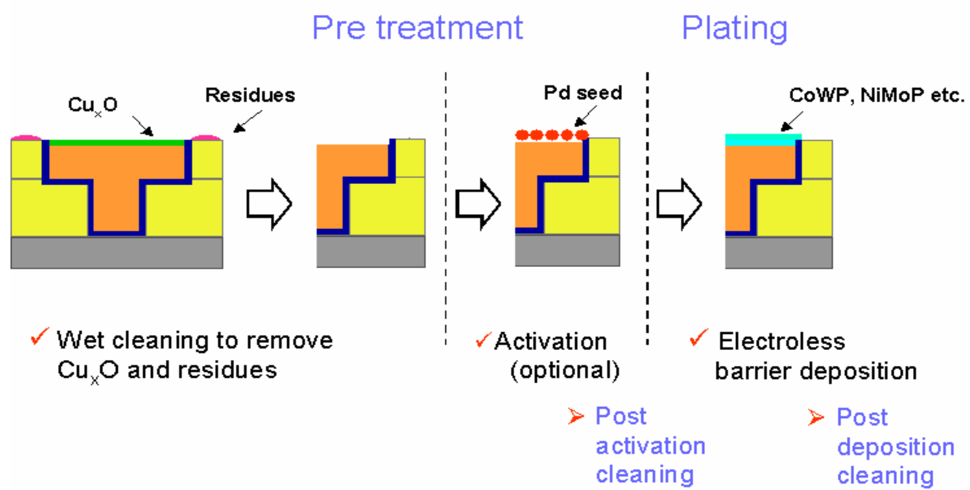

Figure 1-10: Cu film capping layer process.

1 ul of Whole Blood:
0.55 ul Plasma
5 million red blood cells
5,000-10,000 White Blood Cells
200,000-300,000 Platelets
Salts, organics, etc.

Red Blood Cells:
7.5 microns in diameter
No Nucleus
Oxygen Transport

White Blood Cells:
2 main types (granular(3), nongranular(2))
Immune System Function

Patelet:
2-3 microns in diameter
No Nucleus
Blood Clotting

Figure1-11: Whole blood contents.

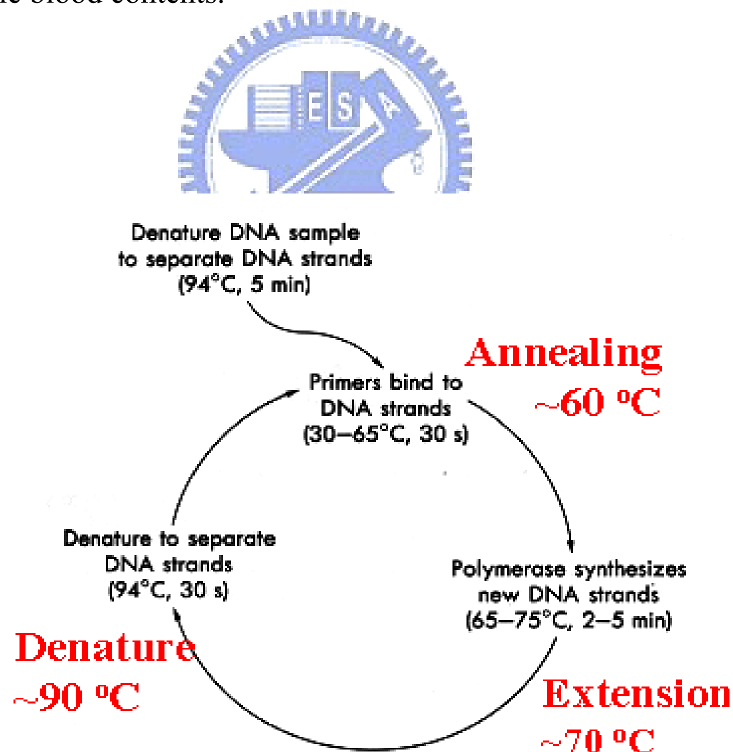

Figure1-12: Polymerase Chain Reaction-process.

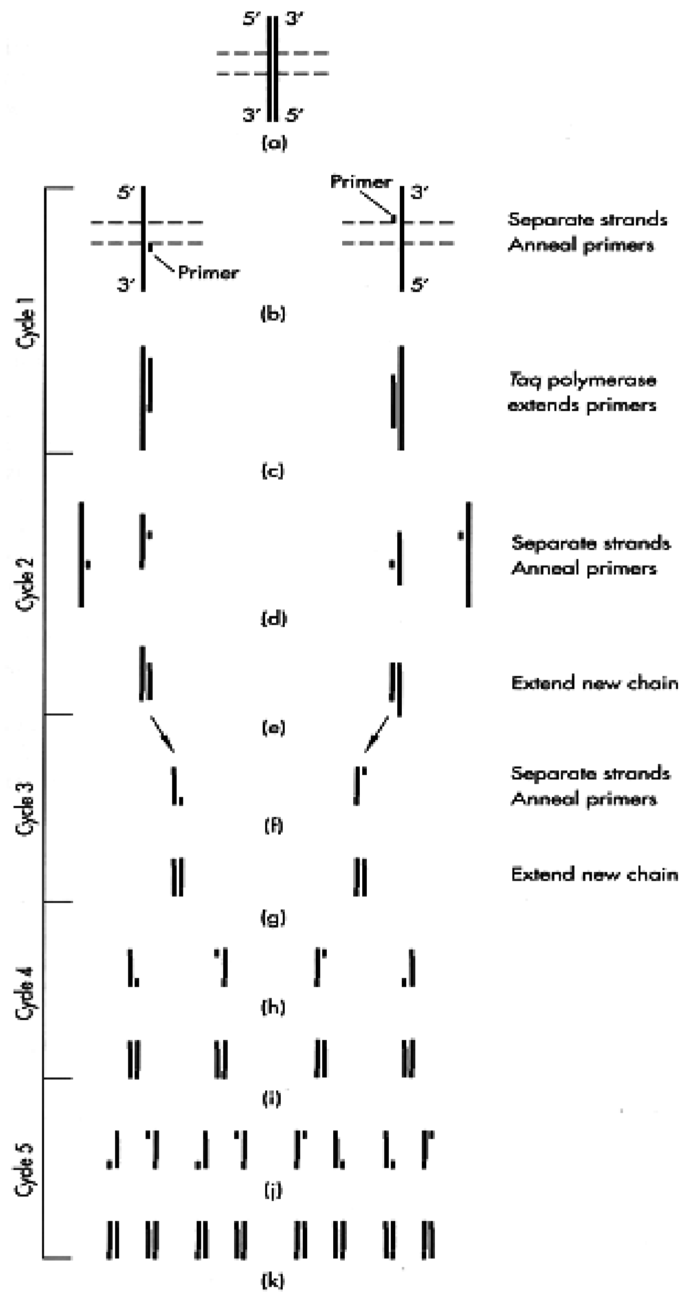

Figure1-13: Polymerase Chain Reaction-amplify mechanism.

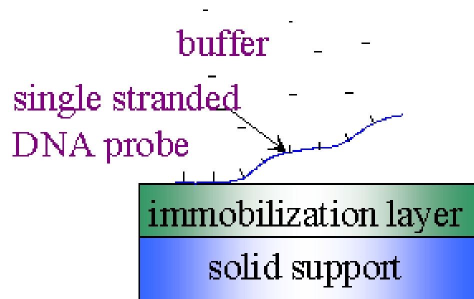

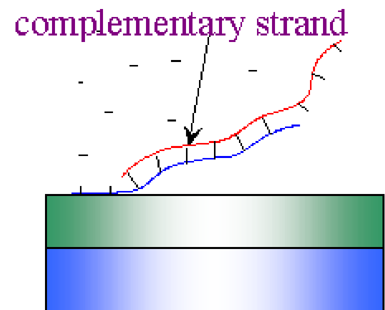

Figure 1-14: DNA hybridization on solid support.

Chapter 2

Comparing Nanoscale Characterization of TaN_x Barrier Thin Films Prepared by NH_3/Ar and N_2/Ar Reactive Gases

Abstract

To obtain high-performance Cu diffusion barriers, we compared the nanoscale characteristics of TaN_X diffusion barrier thin films prepared using RF reactive sputtering with NH_3/Ar and N_2/Ar as reactive gas mixtures. Because the N≡N bond energy of N_2 is 942 kJ/mol and the N−H bond energy of NH_3 is 388 kJ/mol, NH_3 was more reactive than N_2. We used cross-sectional TEM to measure the deposition rates and XPS and AES to obtain the N/Ta ratios of these TaN_X thin films. The crystal morphology and fine nanoscale structure were observed using XRD, bright-field cross-sectional TEM, and TEM diffraction. The use of AFM allowed us to measure the each sample's flatness. The grain size and grain density were determined using plan-view TEM and AFM. We measured the resistivity using a four-point probe. Measurements of the leakage currents of Cu/TaN_X/n^+np^+ diodes, which were subjected to rapid thermal annealing, allowed us to distinguish the thermal stabilities of the TaN_X diffusion barriers. The thermal stabilities of the TaN_X films were dependent predominantly on their crystal structures, and less so on their gas source. Higher N/Ta ratios led to Cu/TaN_X/n^+np^+ diode structures possessing improved thermal stability, but their resistivity increased when this ratio was too high. When the N/Ta ratio was ca. 1, the films exhibited good thermal stability and moderate resistivity.

2-1 Introduction

As the ULSI (Ultra-Large Semiconductor Integration) line width decreases, RC delay becomes a more serious problem. The replacement of aluminum by copper has been proposed for line widths smaller than 0.13 μm because copper improves conductivity and reduces electro-migration.[1] Unfortunately, Cu readily diffuses into Si and, therefore, it influences device performance; for example, the introduction of Cu into Si transistors leads to deep-level doping that influences the minor carrier lifetime and increases the junction leakage current.[2] Preventing Cu from diffusing requires that the diffusion barrier between Si and Cu be increased. The question then arises: What kind of diffusion barrier is most useful? Several researchers have demonstrated that TaN_X provides good performance: it has a relatively high melting temperature and it is thermodynamically stable with respect to Cu. Studies of the effects that various forms of TaN_X have on the prevention of Cu diffusion have revealed that the relative order of stability is TaN[3–6] > Ta_2N[7,8] > Ta[4,6,8–10]. A diffusion barrier's thermal stability can be evaluated through measurements of whether or not Cu can diffuse through it.[3] Such measurement methods include (1) XRD (measuring Cu silicide formation), (2) AES depth profiling (monitoring concentration changes of all atoms), and (3) electrical measurements (e.g., leakage current of $Cu/TaN_X/n^+np^+$ diodes). Because the sensitivity of the latter approach is better than those of the XRD and AES methods, we chose to evaluate the thermal stabilities of TaN_X diffusion barriers through measurements of their electrical properties. Ideally, we wished to develop a thermally stable, low-resistively, high-performance TaN diffusion barrier for Cu processing.

In this study, we characterized TaN_X diffusion barrier thin films on the nanoscale after they had been subjected to RF reactive sputtering with NH_3/Ar or N_2/Ar reactive gas mixtures. We measured the leakage current of $Cu/TaN_X/n^+np^+$

diodes that had been treated through RTA thermal annealing to distinguish the thermal stabilities of the TaN_X diffusion barriers. The thermal stability of a TaN_X film depends predominantly on its crystal structure, but less so on the gas source used. Higher N/Ta ratios lead to $Cu/TaN_X/n^+np^+$ diodes exhibiting superior thermal stability, but the resistivity increases when the ratio is too high. When the N/Ta ratio is ca. 1, the films exhibit good thermal stability and medium resistivity and, therefore, they provide a high performance Cu diffusion barrier.

2-2 Experimental Section

The surfaces of the Si wafers were cleaned through RCA processing. The TaN_x thin films were deposited through RF reactive sputtering using NH_3/Ar or N_2/Ar as the reactive gas mixture. The RF power was fixed at 300 W; sputter base pressure was 5×10^{-7} Torr; the Ar flow rate was 6 SCCM; the operating pressure was 3×10^{-2} Torr; the NH_3/Ar or N_2/Ar flow ratios were 0.075, 0.100, 0.125, 0.150, 0.175, 0.200, 0.225, and 0.300.

RF reactive sputtering was used to grow 25-nm-thick TaN_X films on a diode; in situ deposition of a 60-nm-thick Cu layer was then conducted using different flow ratios of the NH_3/Ar or N_2/Ar gas mixtures. Subsequently, the samples were placed into a vacuum RTA (rapid thermal annealing) machine operated at 450–650 °C for 30 min. After RTA, the samples were removed and their leakage currents were measured using a SONY tektronix 370A operated at an applied potential of –5 V.

2-3 Results and Discussion

Figure 2-1 displays the deposition rates of the TaN_X thin films with respect to different NH_3/Ar or N_2/Ar flowing ratios. The growth rate underwent a step change[11] from 50.67 to 25.0 nm/min; the step change point occurred at an NH_3/Ar flow ratio of 0.17. The N_2/Ar curve also features a step change, from 60.0 to 23.0 nm/min; this step change point occurred at 0.175. Because the N≡N bond energy of N_2 is 942 kJ/mol and the N－H bond energy of NH_3 is 388 kJ/mol, NH_3 is more reactive than N_2.[12] We found that NH_3 displayed a lower initial deposition rate than did N_2, presumably because NH_3 was more reactive [we also observed that the N/Ta ratio for NH_3 was higher than that for N_2 at low NH_3/Ar or N_2/Ar flow ratios (shown in Figure 2-4)] and, hence, its nitrogen sputtering rate was lower (the higher nitrogen ratio of a target the lower sputtering rate of deposition).[11] On the other hand, toward the end of the sputtering process, N_2 mediated a lower deposition rate than did NH_3, presumably because N_2 gas is more nitrogen-rich than is NH_3 gas [we also observed that the N/Ta ratio for N_2 was higher than that for NH_3 at high NH_3/Ar or N_2/Ar flow ratios (shown in Figure 2-4)]. Figure 2-2 presents Ta 4f XPS data obtained from the TaN_X thin films grown at different NH_3/Ar flow ratios. Increasing the NH_3/Ar flow ratio from 0.075 to 0.300 caused the binding energy of the Ta $4f_{7/2}$ peak to increase from 22.0 to 22.8 eV (Figure 2-2A), a total increase of 0.8 eV. Similarly, when the N_2/Ar flow ratio was increased from 0.075 to 0.300 the binding energy of the Ta $4f_{7/2}$ peak increased from 22.3 to 23.5 eV, a total increase of 1.2 eV. The shift in these Ta 4f7/2 peaks to higher binding energies as the NH_3/Ar or N_2/Ar flow ratios increased imply that the nitrogen content increased in the TaN_X thin films.[13, 14] From these data we deduce that the use of N_2/Ar led to TaN_X thin films having richer nitrogen contents than did the use of NH_3/Ar at high NH_3/Ar or N_2/Ar flow ratios. Figure 2-3 presents the N_{1S} XPS data

obtained for the growth of the TaN_X thin films at different NH_3/Ar or N_2/Ar flow ratios. The N_{1S} peak became more intense upon increasing the NH_3/Ar or N_2/Ar flow ratios; the nitrogen content in the TaN_X thin films increased up to a constant value at high flow ratios. Figure 2-4 presents the N/Ta ratios obtained at different NH_3/Ar or N_2/Ar flow ratios using the data calculated from the ESCA tools from Figure 2-2. Because NH_3 is more reactive than N_2, the use of NH_3 led to higher N/Ta ratios at low flow ratios. Besides, N_2 is more nitrogen-rich than NH_3, the use of N_2 led to higher N/Ta ratios at high flow ratios.[12] The use of NH_3/Ar and N_2/Ar both led to saturated N/Ta ratios—1.26 and 1.40, respectively—at high flow ratios.

Figure 2-5 presents the XRD data obtained from the TaN_X thin films grown at different NH_3/Ar and N_2/Ar flow ratios. When the NH_3/Ar flow ratio increased (Figure 2-5A), the structures of the TaN_X thin films changed from BCC－Ta (at flow ratios of 0.075 and 0.100) to FCC－TaN (from 0.125 to 0.250) to nanocrystalline－TaN (at 0.300).[4,13–15] When the N_2/Ar flow ratio increased (Figure 2-5B), the structures of the TaN_X thin films also changed from BCC－Ta (from 0.075 to 0.150) to FCC－TaN (from 0.175 to 0.200) to nanocrystalline－TaN (from 0.225 to 0.300).[4,13,14,15] The transformation from BCC－Ta to FCC－TaN occurred at a lower NH_3/Ar flow ratio from 0.100 to 0.125 than that observed when using N_2/Ar from 0.150 to 0.175, because NH_3/Ar provided a more reactive gas source at low flow ratios (shown in Figure 2-4). On the other hand, the transformation from FCC－TaN to nanocrystalline－TaN occurred at a lower N_2/Ar flow ratio from 0.200 to 0.225 than that observed when using NH_3/Ar from 0.250 to 0.300, because N_2/Ar provided a richer nitrogen source at high flow ratios (shown in Figure 2-4). Figure 2-6A presents the bright-field cross-sectional TEM images and diffraction patterns recorded at

different NH_3/Ar flow ratios. When the NH_3/Ar flow ratio was 0.075, the TaN thin film possessed a BCC polycrystalline structure, as verified by the ring pattern displayed in Figure 2-6A(a); the bright-field cross-sectional TEM images displayed a columnar structure. When the NH_3/Ar flow ratio increased to 0.175, the TaN thin film possessed a FCC polycrystalline structure, that we also verified from the ring pattern in Figure 2-6A(b); the bright-field cross-sectional TEM image indicates a closer columnar structure, which suggests that a preferred orientation existed in this film [16]. In Figure 2-5A(e), the preferred orientation was (111). When the NH_3/Ar flow ratio reached 0.300, the TaN thin film became nanocrystalline, again verified from the ring pattern presented in Figure 2-6A(c). The bright-field cross-sectional TEM image also displays a nanocrystalline structure. In Figure 2-5A(i), we observe dispersive peaks. Figure 2-6B displays the corresponding bright-field cross-sectional TEM images and diffraction patterns of the films prepared at different N_2/Ar flow ratios. When N_2/Ar flowing ratio was 0.075, the TaN thin film had a BCC polycrystalline structure, as indicated by the ring pattern in Figure 2-6B(a) and the bright-field cross-sectional TEM image of a columnar structure. When the N_2/Ar flowing ratio increased to 0.175, the TaN thin film became FCC polycrystalline, as verified by the ring pattern in Figure 2-6B(b); the bright-field cross-sectional TEM image displays a closer columnar structure, suggesting that a preferred orientation existed.[16] In Figure 5B(e), the preferred orientation was (111). When the N_2/Ar flow ratio reached 0.300, the TaN thin film became nanocrystalline in structure, as indicated by the ring pattern in Figure 2-6B(c) and the bright-field cross-sectional TEM image. In Figure 2-5B(i) we observe dispersive peaks. From Figures 2-6A(a) and 2-6B(a) we observe that the TEM ring pattern of TaN was more disconnected—i.e., the grain size was larger[16]—when using NH_3/Ar. The growth of larger TaN crystals when using NH_3/Ar

is also evident in the bright-field cross-sectional TEM images in Figures 2-6A(c) and 2-6B(c). The bright-field plan-view TEM images obtained when using different NH_3/Ar flow ratios (Figure 2-7A) indicate that when flow ratios increased (from 0.075 to 0.175 to 0.300) the grain sizes decreased (from 24.55 to 14.15 to 9.25 nm, respectively). The corresponding images in Figure 2-7B indicate that when the N_2/Ar flow ratio increased from 0.075 to 0.175 to 0.300, the grain sizes decreased from 22.55 to 11.76 to 6.86 nm, respectively. A comparison of Figures 2-7A and 2-7B indicates that the grain sizes of the TaN_X thin films were larger when using the NH_3/Ar gas mixture. Figure 2-8 presents AFM data for the TaN_X thin films. Irrespective of using NH_3/Ar or N_2/Ar for the growth of the TaN_X thin films, the grain sizes decreased upon increasing the flow ratio; these results are consistent with those presented in Figure 2-7.[8] We used these AFM data to calculate the relationships between the grain densities and both the NH_3/Ar and N_2/Ar flow ratios (Figure 2-9). The TaN_X grain densities were higher and the grain sizes were smaller when using N_2/Ar as the gas mixture. When the flow ratio was above a critical pressure, the TaN_X grain density increased rapidly when using either NH_3/Ar or N_2/Ar.

Figure 2-10 displays the resistivity of the films with respect to the NH_3/Ar or N_2/Ar flow ratios. The resistivity increased gradually when the NH_3/Ar or N_2/Ar flow ratios increased. The resistivities underwent large increases when the NH_3/Ar and N_2/Ar flow ratios were above the critical pressure because higher nitrogen contents would lead to more nitrogen atoms existing in the vacancies next to Ta atoms, which would lead to a decrease in crystal order. In addition, the resistivity was larger when using N_2/Ar for the growth of the TaN_X thin films, presumably because the oxygen content was slightly higher at low N_2/Ar flow ratios and because the nitrogen content was greater at a high N_2/Ar flow ratio relative to that of NH_3/Ar. The resistivities of

the TaN_X films prepared below the critical pressure ranged from 130 to 350 μΩ-cm; these values are close to those of the reference data (from 130 to 250 μΩ-cm).[11] Figure 2-11 displays the complete structure of a Cu/TaN_X (25 nm)/n^+np^+ sample. Figure 2-12A presents the characteristic I–V curve of the Cu/$TaN_{0.987}$ (25 nm)/n^+np^+ sample obtained using NH_3/Ar as the reactive gas mixture. From Figure 2-12A(a) we observe that prior to thermal treatment the leakage current was just –0.5 μA at an applied potential of –5 V. After thermal treatment at 500 °C, the leakage current had increased slightly to –2.5 μA at the same applied voltage [Figure 2-12A(b)], suggesting that the Cu/$TaN_{0.987}$ (25 nm)/n^+np^+ sample retained its fine structure. After thermal treatment at 550 °C, the leakage current increased to –15 μA at an applied potential of –5 V [Figure 2-12A(c)], suggesting that some Cu had diffused through the TaN_X barrier layer and into the n^+np^+ diode. After thermal treatment at 600 °C, the leakage current increased to –1220 μA at this applied voltage [Figure 2-12A(d)], suggesting that all of the Cu had diffused through the TaN_X barrier layer and into the n^+np^+ diode; i.e., the TaN_X layer failed as a diffusion barrier. We defined the TaN_X diffusion barrier's thermal capability to be 500 °C (leakage current small than 3μA).[3,17] Figure 2-12B presents the corresponding I–V characteristic curve of the Cu/$TaN_{1.134}$ (25 nm)/n^+np^+ sample prepared using N_2/Ar as the reactive gas mixture; in this case, the TaN_X diffusion barrier's thermal capability was 500 °C.

Table 2-1 summarizes the highest thermal stability temperatures of Cu/TaN_X/n^+np^+ samples with 0.075,0.175 and 0.300 NH_3/Ar or N_2/Ar flow ratio. The corresponded TaN_X thin films structures for 0.075,0.175 and 0.300 NH_3/Ar or N_2/Ar flow ratio were BCC－Ta, FCC－TaN, and nanocrystalline－TaN (shown in Figure 2-5). Both of NH_3/Ar and N_2/Ar have the same TaN_X thin films structures that would have the same thermal stability temperatures. Irrespective of using NH_3/Ar or N_2/Ar

as the reactive gas, the temperature of highest thermal stability for the TaN_X diffusion barriers increased upon increasing the N/Ta ratio,[3,8,9,13,14] presumably because of the increase in the grains' boundary diffusivity.

2-4 Conclusions

Copper has been proposed to replace aluminum for the preparation of ULSI line widths below 0.13 μm, but it is necessary to incorporate a high-performance Cu diffusion barrier. In this study, we monitored the effects on the deposition rate, composition, crystal structure, and resistivity of TaN_X films as a function of their reactive gas source and gaseous flow ratio. As the flow ratio of the reactive gases increased, the structures of the TaN_X films changed from BCC－Ta to FCC－TaN to nanocrystalline－TaN. The growth of TaN_X films through RF sputtering using NH_3/Ar gas mixtures led to larger grain sizes and lower resistivities. The thermal stabilities of TaN_X films were dependent predominantly on their crystal structure, and less so on their gas source. Higher N/Ta ratios led to improved thermal stabilities of Cu/TaN_X/n^+np^+ diode structures, but the resistivity increased when the ratio was too high. At an N/Ta ratio of ca. 1, the films exhibited good thermal stability and moderate resistivity and behaved as high-performance Cu diffusion barriers.

References

[1]. C. Y. Chang and S. M. Sze, ULSI Technology, McGraw-Hill, New York (1996) 371.

[2]. Y. Shacham`-Diamand, J. Li, J. O. Olowlafe, S.,Russel, Y.,Tamou and J.W. Mayer, Proc 9 Bienn Univ. Gov. Ind. Microelectron Symp. Publ by IEEE Service Center, Piscataway, NJ (IEEE cat. n 91ch3027-0) 210.

[3]. M. T. Wang, Y. C. Lin and M. C. Chen, J. Electrochem. Soc. 135 (1998) 2538.

[4]. A. Noya, K. Sasaki and Initial. Takeyama, Jpn. J. Appl. Phys. 32 (1993) 911.

[5]. J. O. Olowolafe and C. J. Mogab, J. Appl. Phys. 72 (1992) 4099.

[6]. M. Stavrev, C. Wenzel, A. Möller and K. Drescher, Appl. Surf. Sci. 91 (1995) 257.

[7]. T. Oku, E. Kawakami, M. Uekuo, K. Takahiro, S. Yamaguchi and M. Murakami, Appl. Surf. Sci. 99 (1996) 265.

[8]. K. Holloway, P. M. Fryer, C. Cabral, Jr., J. M. E. Harper, P. J. Bailey, and K. H. Kelleher, J. Appl. Phys 71 (1992) 5433.

[9]. E. Kolawa, J. S. Chen, J. S. Raid, P. J. Pokela and M. A. Nicolet, J. Appl. Phys. 70 (1991) 1369.

[10]. L. A. Clevenger, N. A. Bojarczuk, K. Holloway and J. M. E. Harper, J. Appl. Phys. 73 (1993) 300.

[11]. X. Sun, E. Kolawa, J. S. Chen, J. S. Reid and M.-A. Nicolet, Thin Solid Films 236 (1993) 347.

[12]. T. Okamoto, M. Shimizu, A. Ohsaki, Y. Mashiko, K. Tsukamoto, T. Mastsukawa, and S. Nagao, J. Appl. Phys. 62 (1987) 4465.

[13]. K. Sasaki, A. Noya and T. Umezawa, Jpn. J. Appl. Phys. 29 (1990) 1043.

[14]. M. Takeyama, A. Noya, T. Sase and A. Ohta, J. Vac. Sci. Technol. B 14 (1996)

674.

[15]. K. Wakasugi, M. Tokunaga, T. Sumita, H. Kubota, M. Nagata and Y. Honda, Physica B 239 (1997) 29.

[16]. L. J. Chen, Material TEM (1990) 73.

[17]. M. H. Tsai and S. C. Sun, C. E. Tsai, S. H. Chuang, and H. T. Chiu, J. Appl. Phys. 79 (1996) 6932.

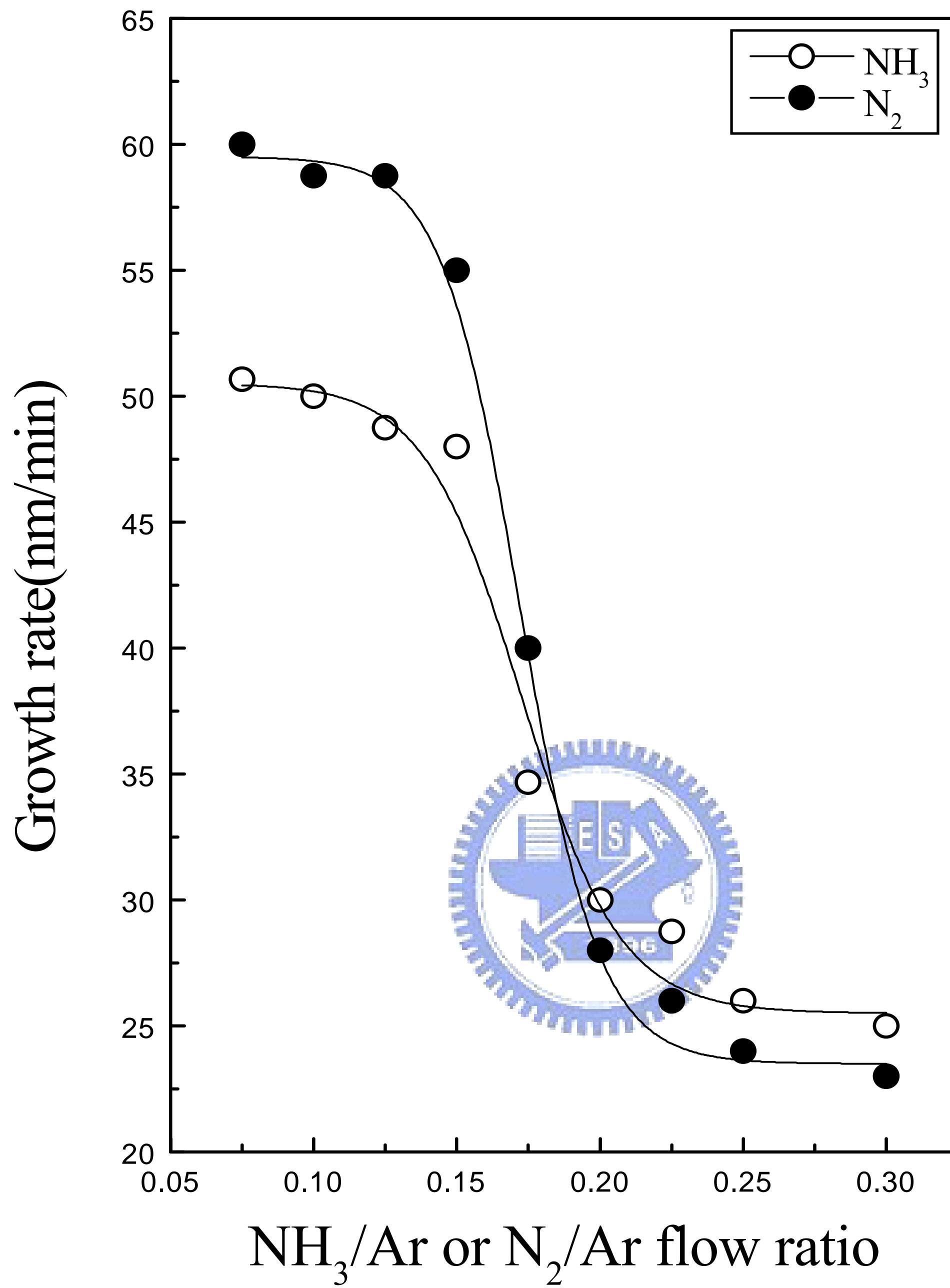

Figure 2-1: Deposition rates of TaN_X thin films with respect to different NH_3/Ar and N_2/Ar flow ratios.

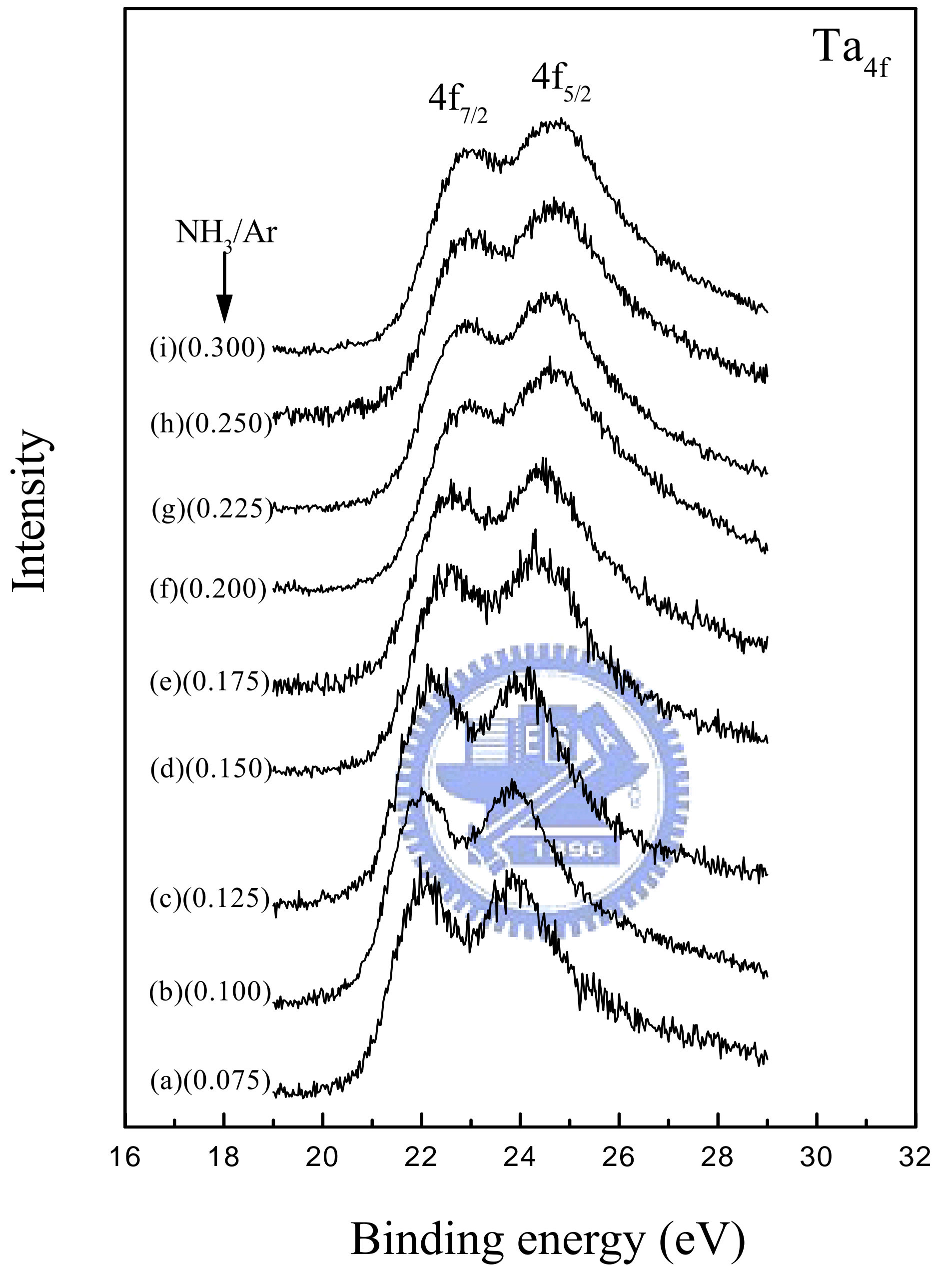

Figure 2-2(A): Ta 4f XPS data from TaN_X thin films grown at different NH_3/Ar flow ratios.

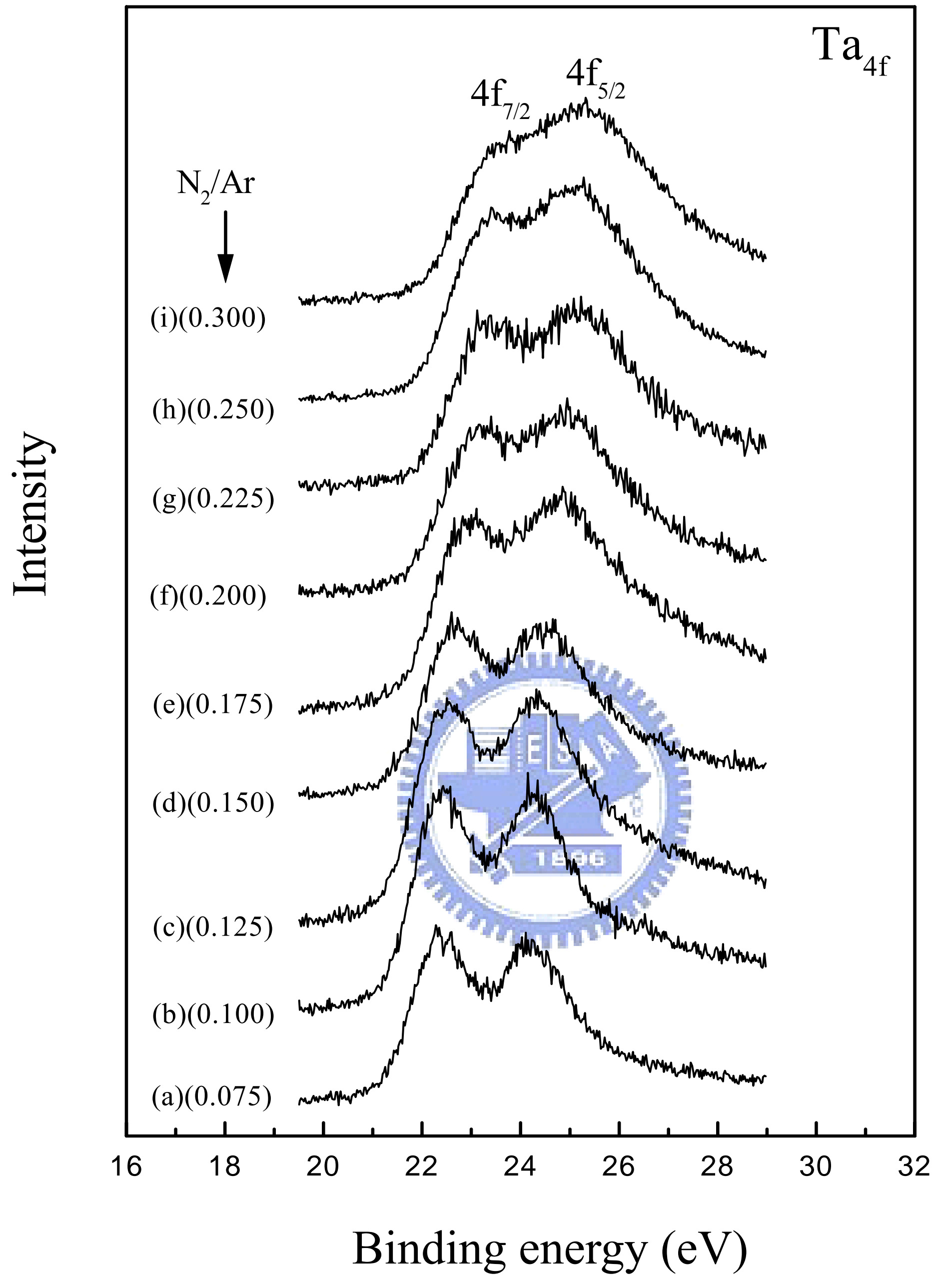

Figure 2-2(B): Ta 4f XPS data from TaN_X thin films grown at different N_2/Ar flow ratios.

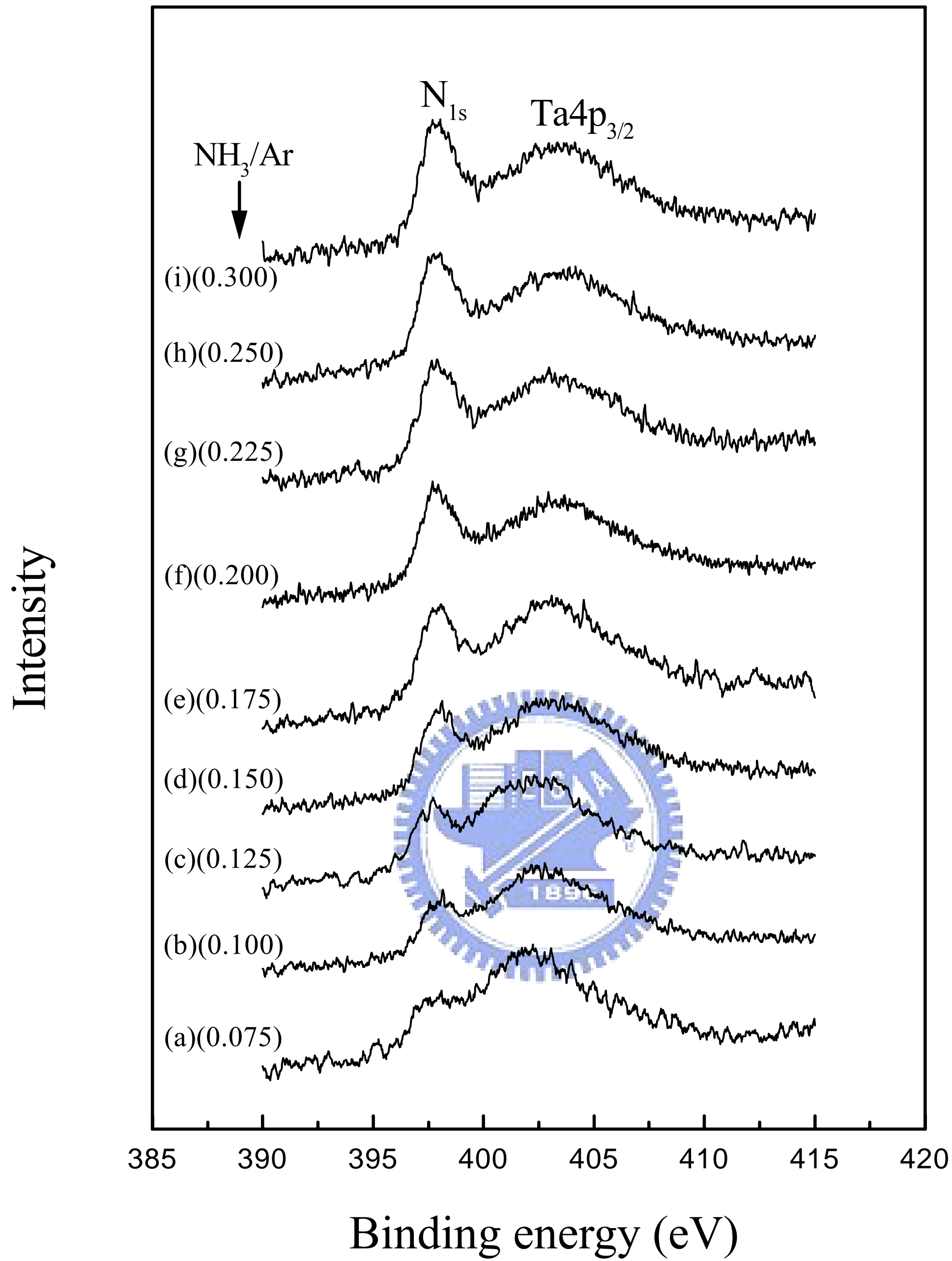

Figure 2-3(A): N_{1S} XPS data from TaN_X thin films grown at different NH_3/Ar flow ratios.

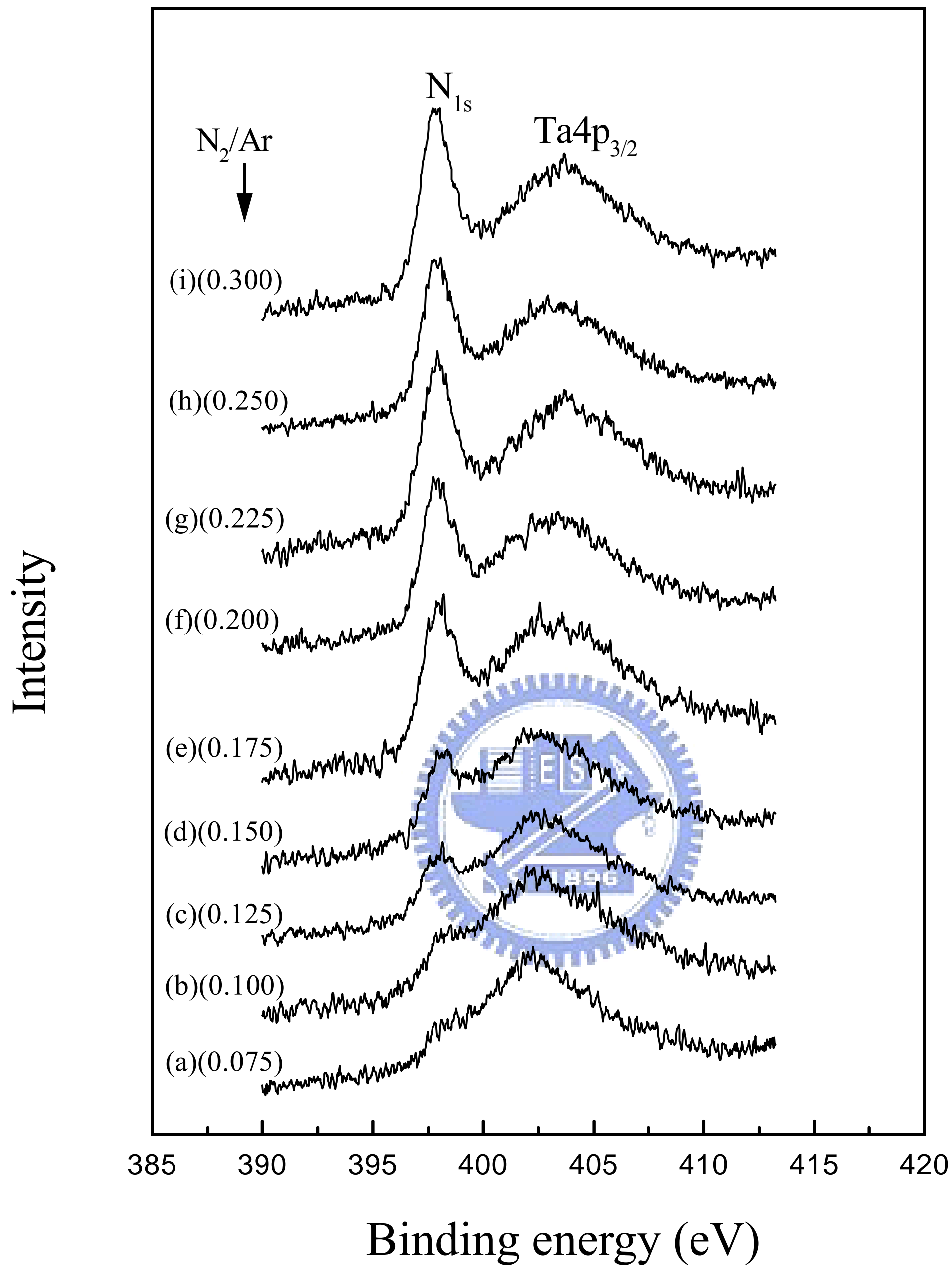

Figure 2-3(B): N_{1S} XPS data from TaN_X thin films grown at different N_2/Ar flow ratios.

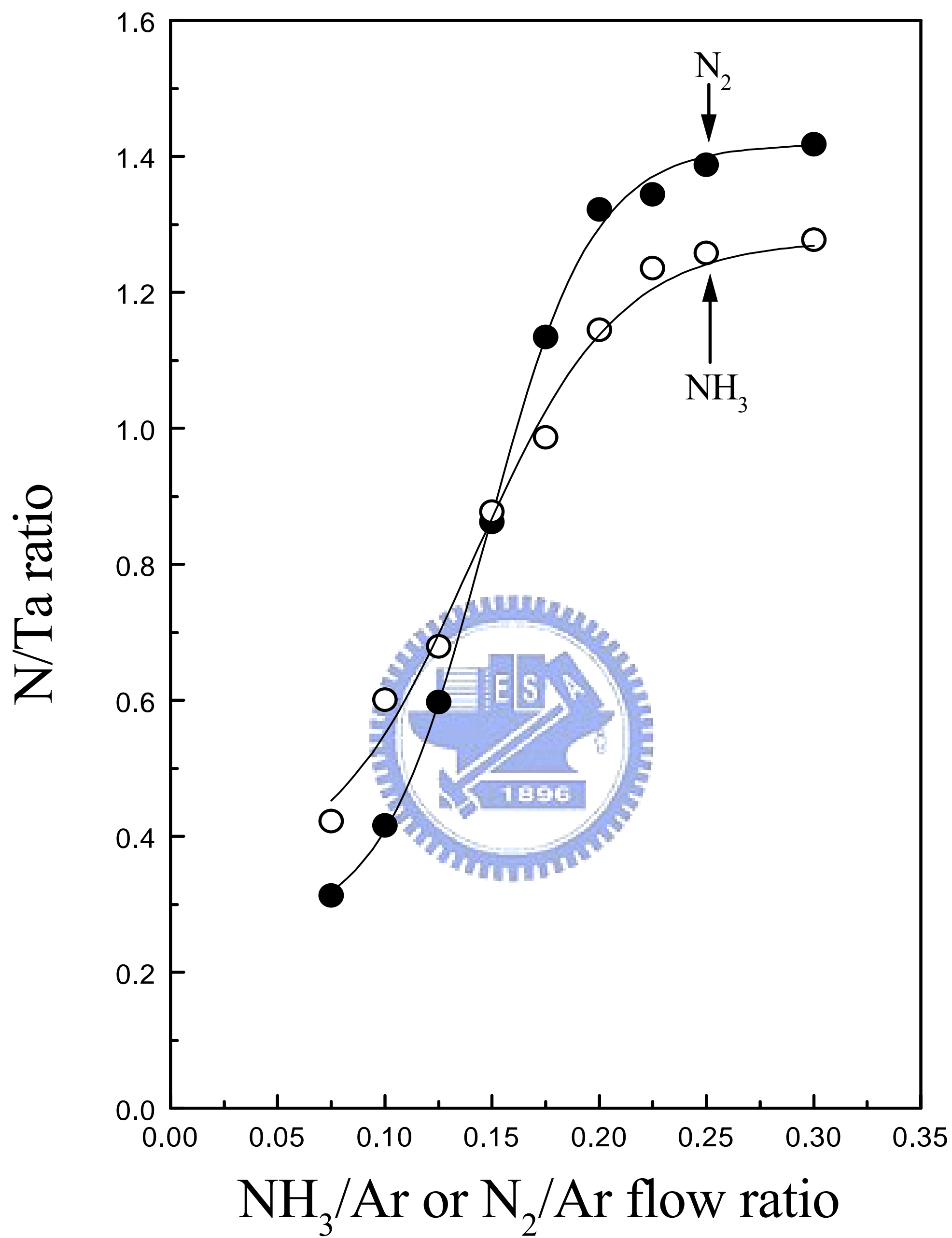

Figure 2- 4: N/Ta ratios obtained at different NH_3/Ar and N_2/Ar flow ratios.

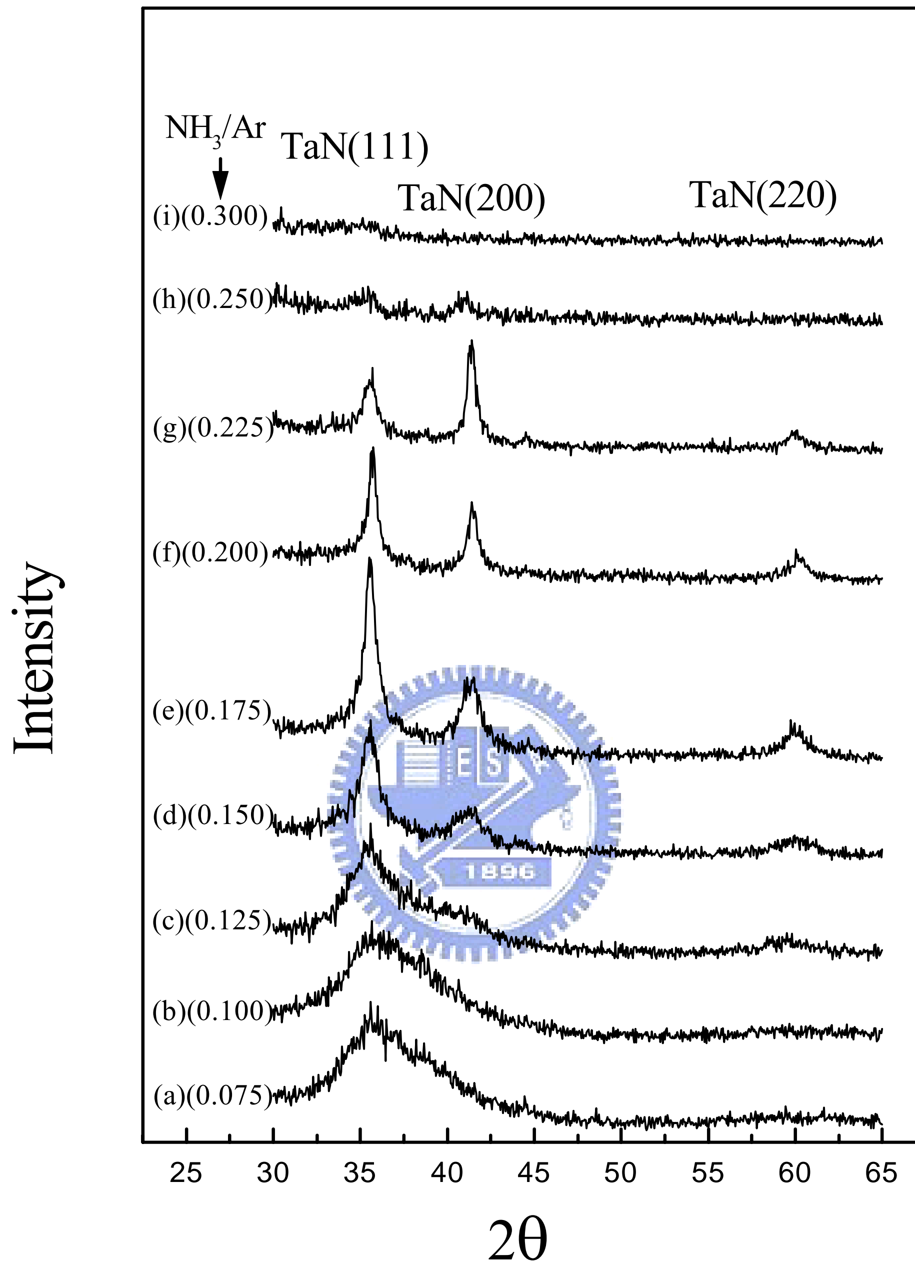

Figure 2- 5(A): XRD data from TaN_X thin films grown at different NH_3/Ar flow ratios.

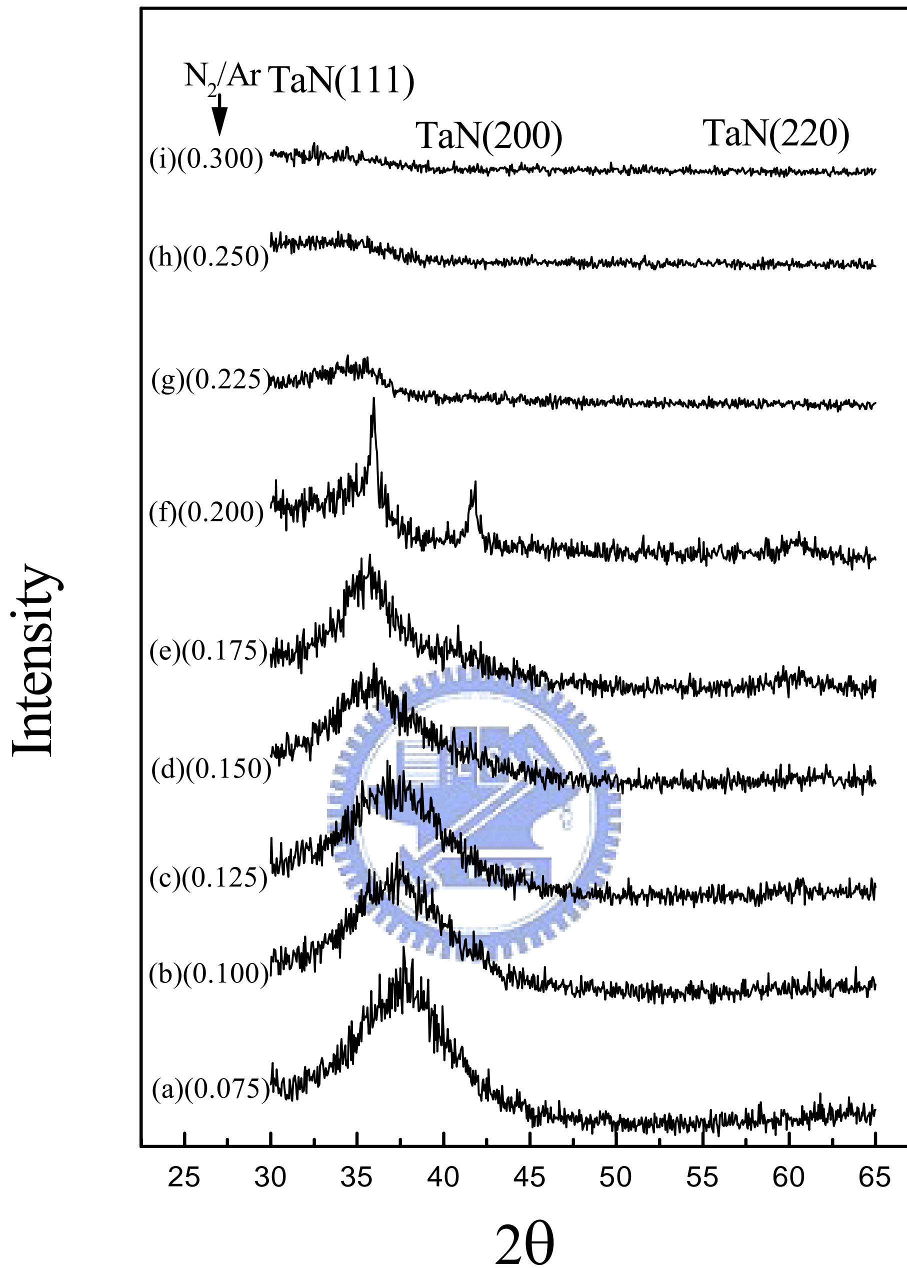

Figure 2- 5(B): XRD data from TaN_X thin films grown at different N_2/Ar flow ratios.

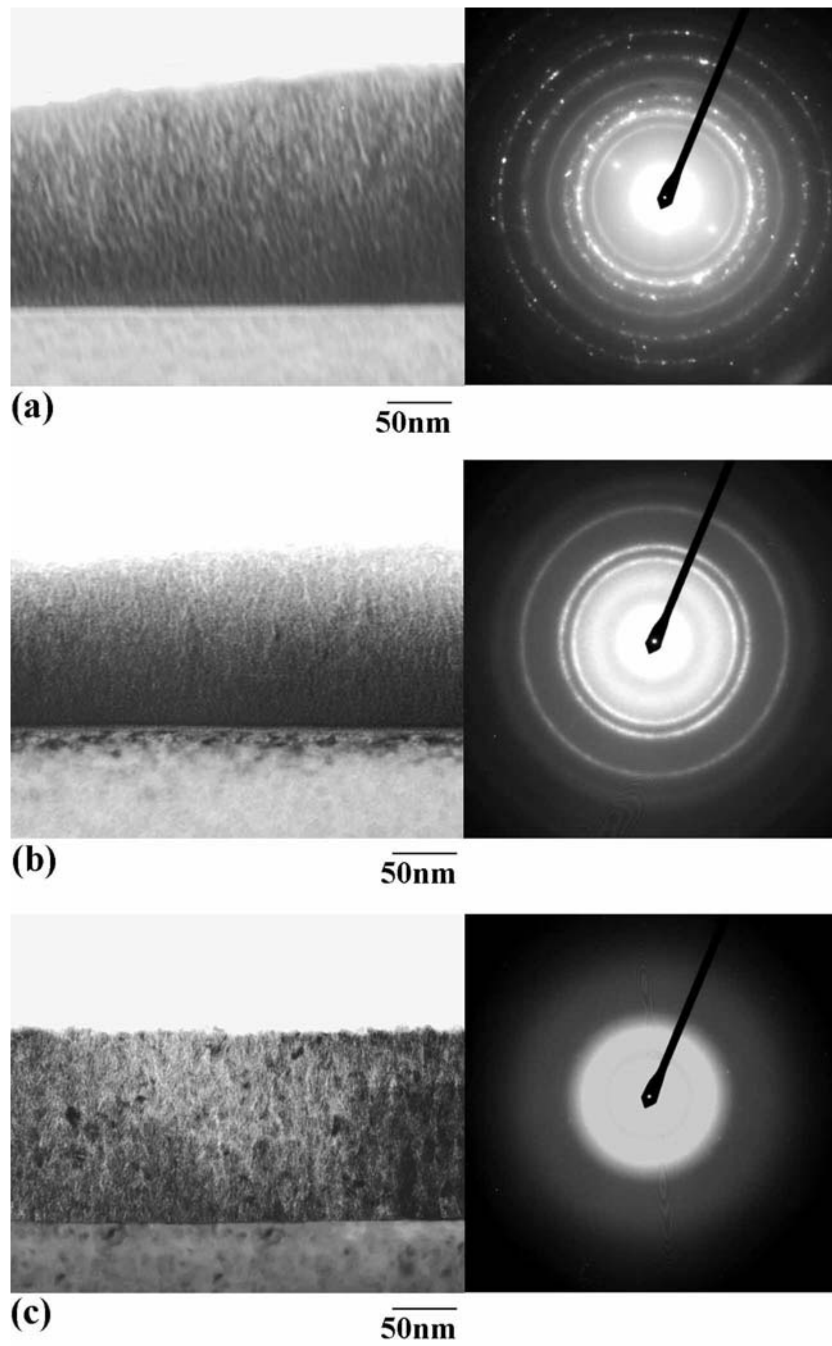

Figure 2-6(A): Bright-field cross-sectional TEM images and diffraction patterns of TaN_X thin films grown at different NH_3/Ar flow ratios (a) 0.075; (b) 0.175; (c) 0.300.

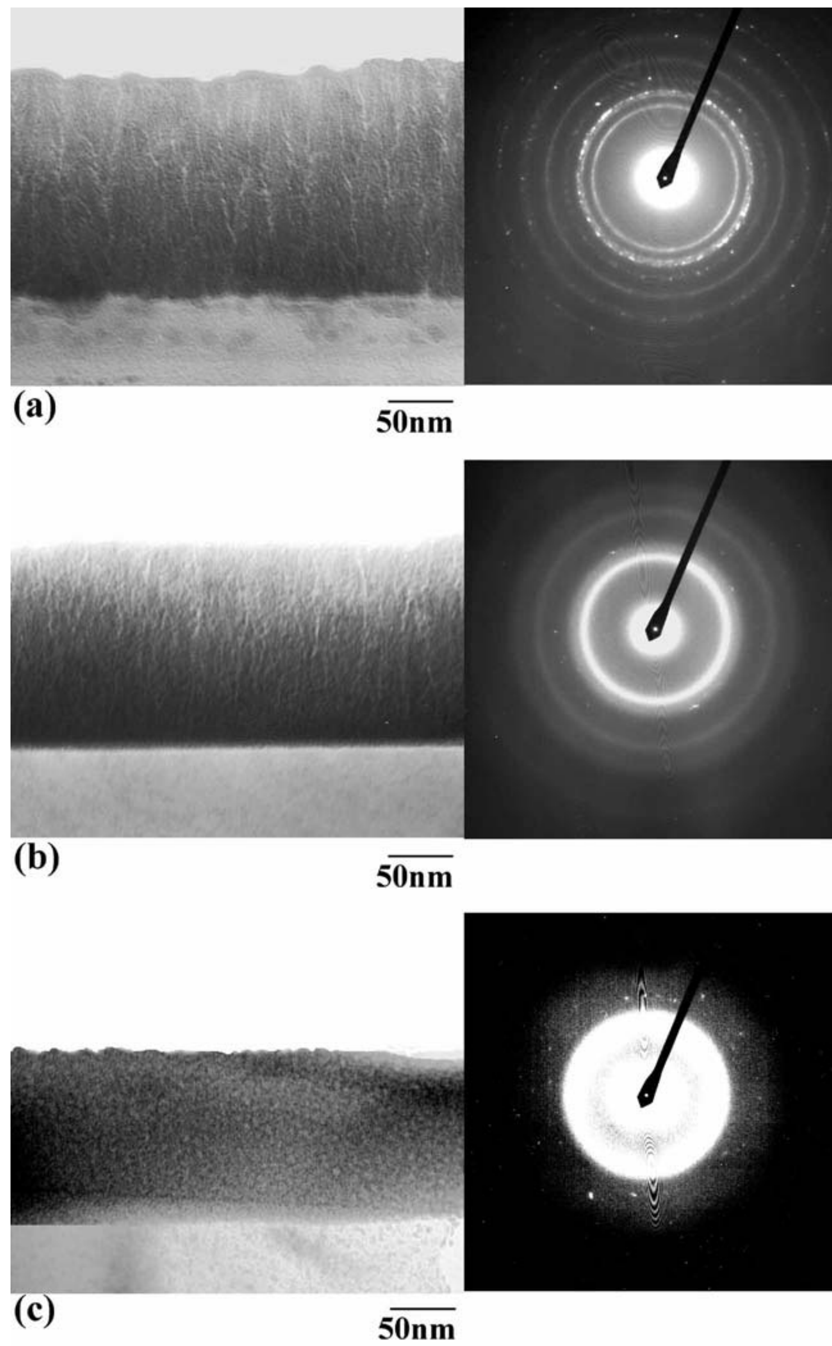

Figure 2-6(B): Bright-field cross-sectional TEM images and diffraction patterns of TaN_X thin films grown at different N_2/Ar flow ratios (a) 0.075; (b) 0.175; (c) 0.300.

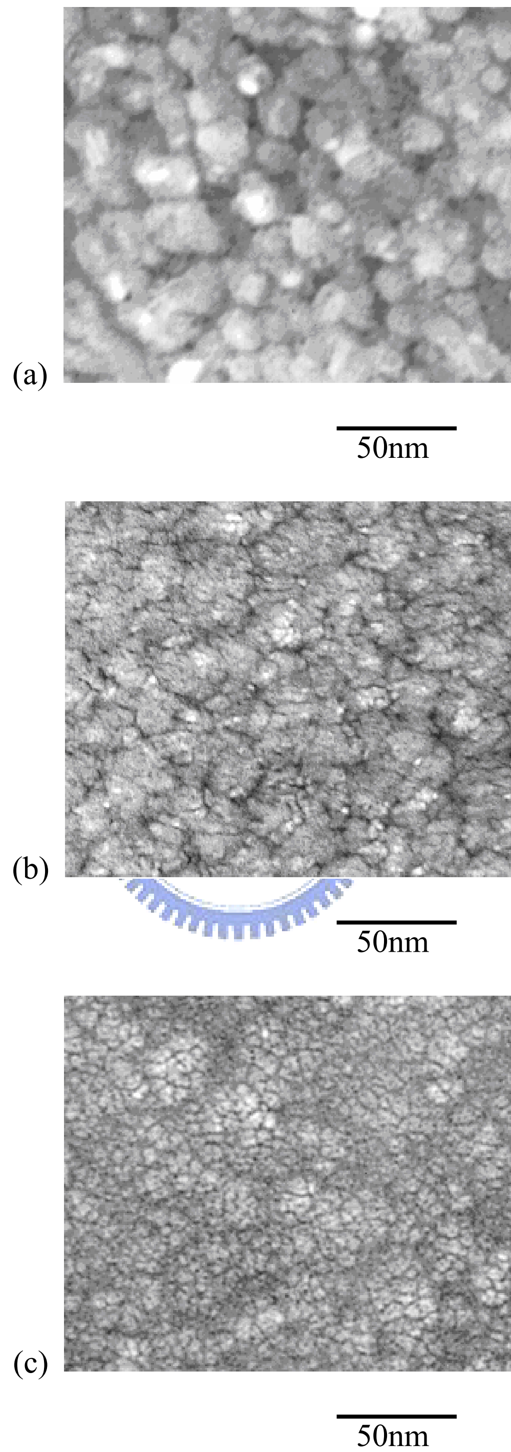

Figure 2-7(A): Bright-field plan-view TEM images of TaN_X thin films grown at different NH_3/Ar flow ratios (a) 0.075; (b) 0.175; (c) 0.300.

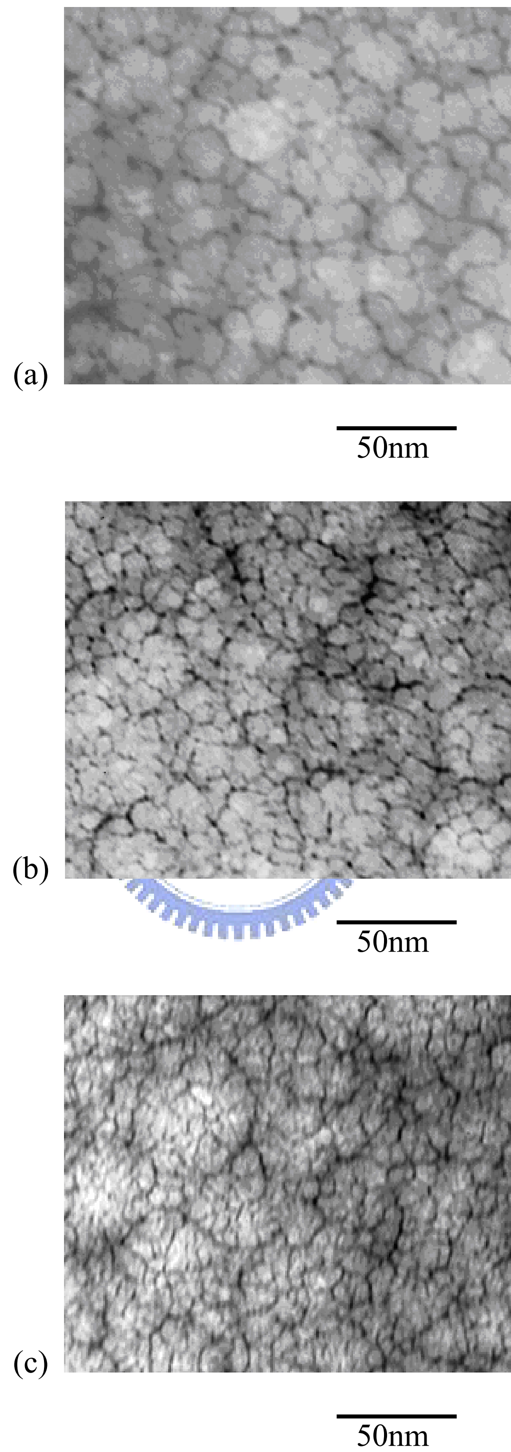

Figure 2-7(B): Bright-field plan-view TEM images of TaN_X thin films grown at different N_2/Ar flow ratios (a) 0.075; (b) 0.175; (c) 0.300.

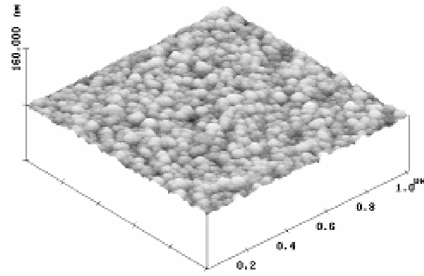

(a)

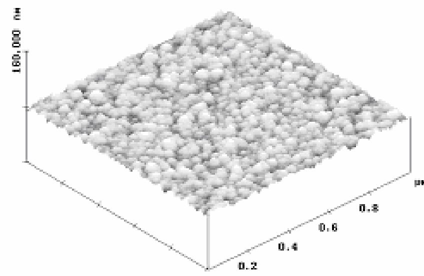

(b)

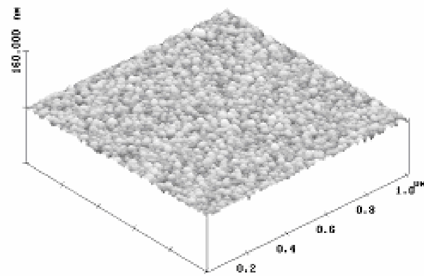

(c)

Figure 2-8(A): AFM data for TaN_X thin films grown at different NH_3/Ar flow ratios (a) 0.075; (b) 0.175; (c) 0.300.

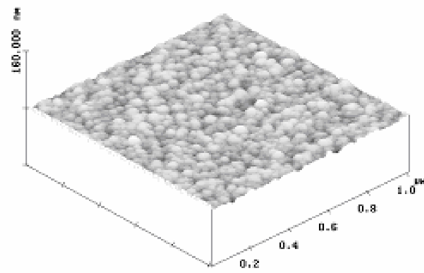

(a)

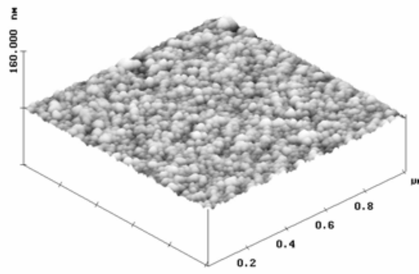

(b)

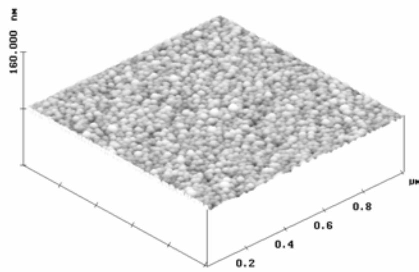

(c)

Figure 2-8(B): AFM data for TaN_X thin films grown at different N_2/Ar flow ratios (a) 0.075; (b) 0.175; (c) 0.300.

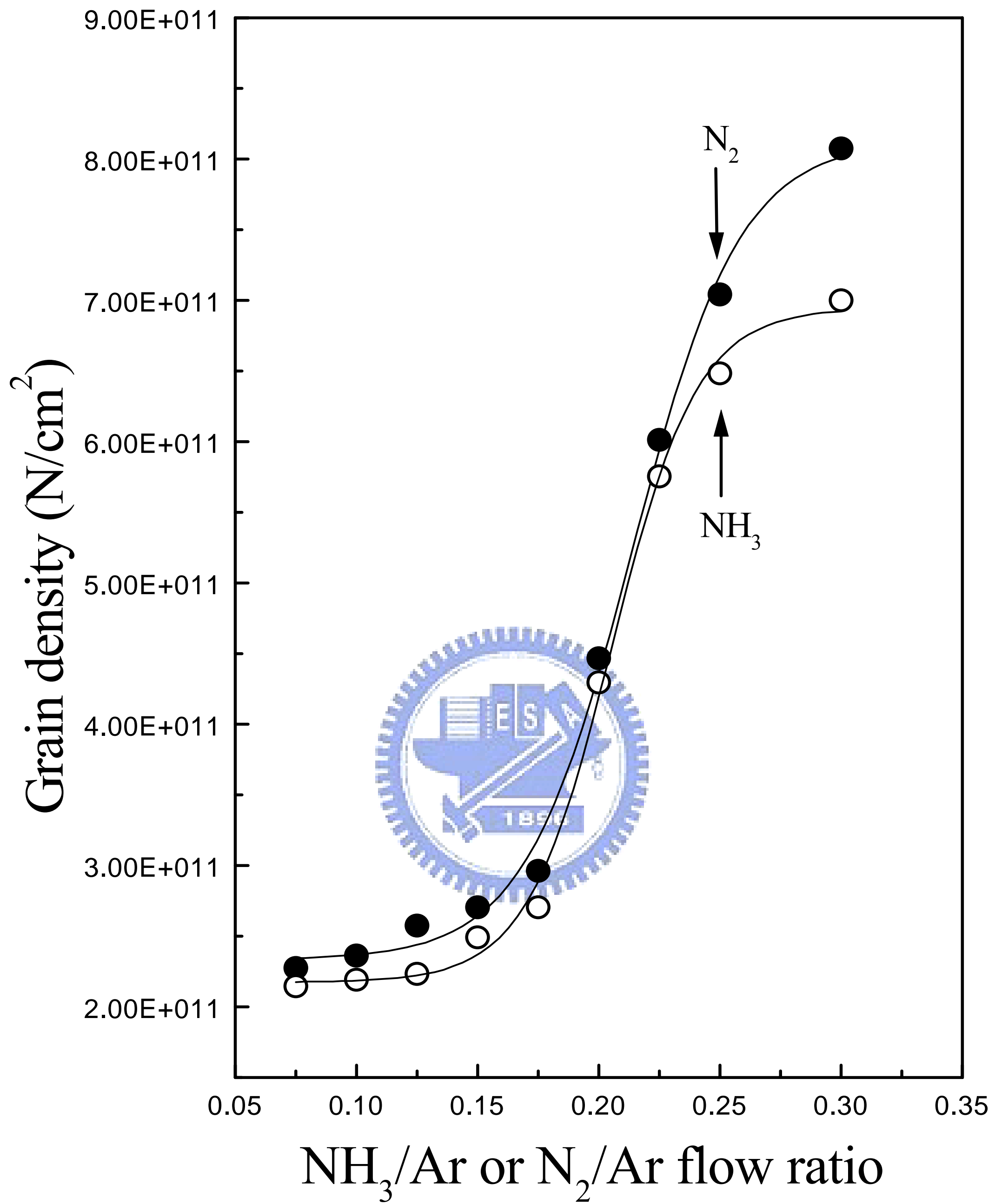

Figure 2-9: Grain densities of TaN_X thin films grown at different NH_3/Ar and N_2/Ar flow ratios.

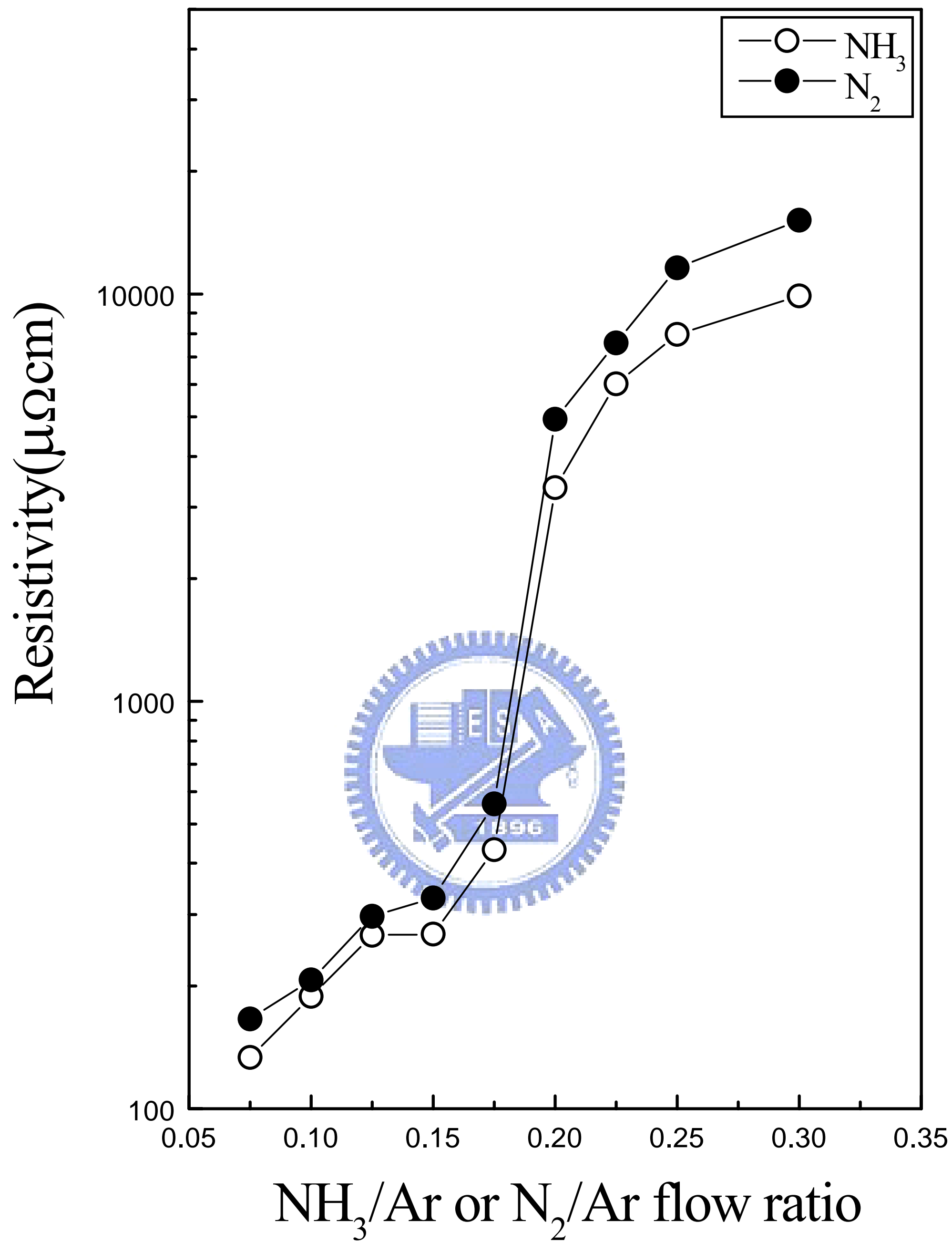

Figure 2-10: Resistivities of TaN_X thin films grown at different NH_3/Ar and N_2/Ar flow ratios.

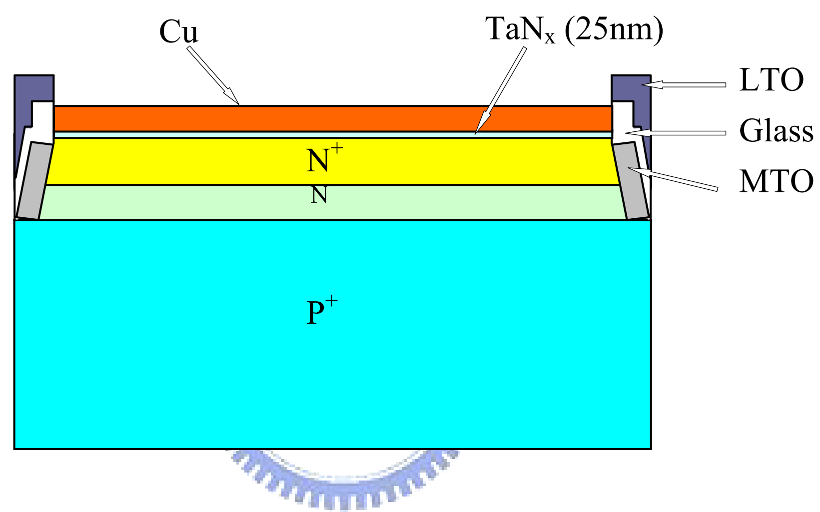

Figure 2-11: Complete structure of a Cu/TaN_X (25 nm)/n^+np^+ sample.

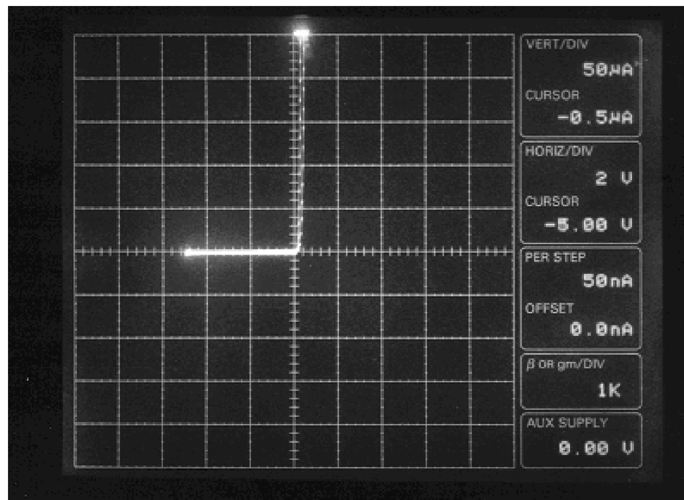

(a)

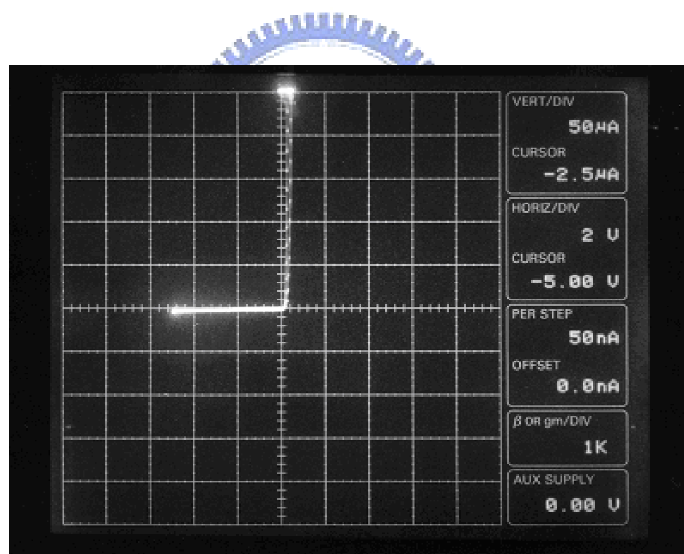

(b)

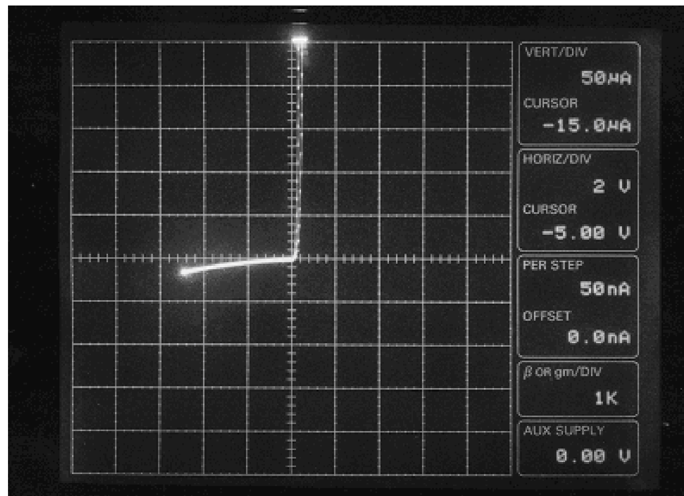

(c)

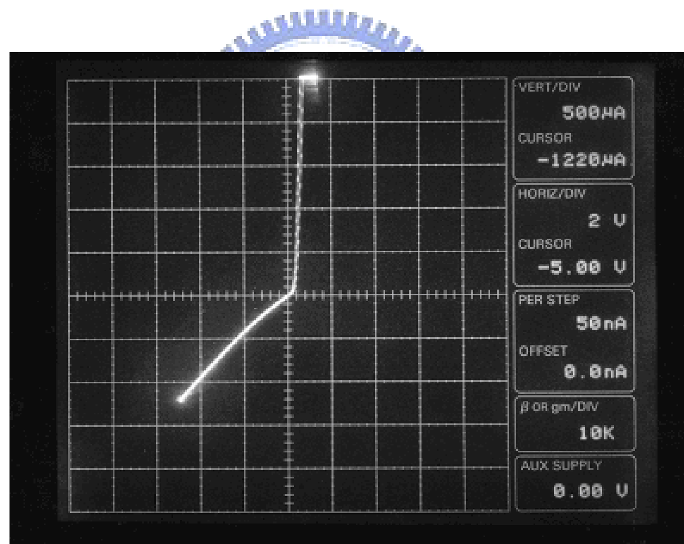

(d)

Figure 2-12(A): Characteristic I–V curves of $Cu/TaN_{0.987}/n^{+}np^{+}$ samples prepared using NH_3/Ar as the reactive gas mixture (a) Before thermal treatment and (b–d) after thermal treatment at (b) 500, (c) 550, and (d) 600 °C.

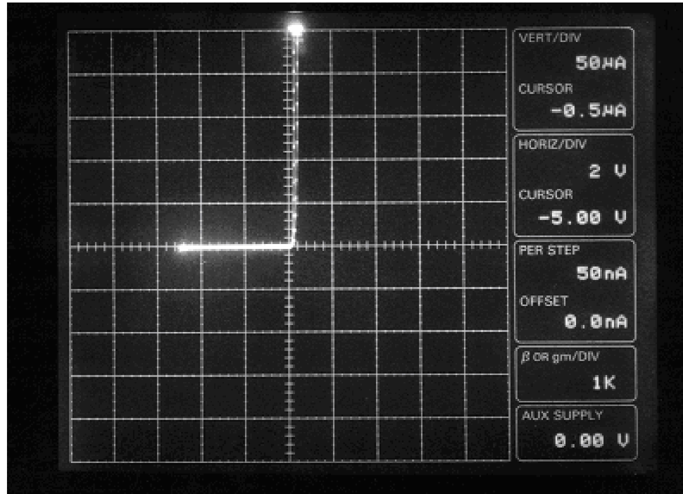

(a)

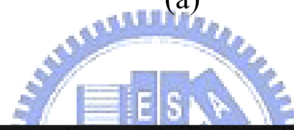

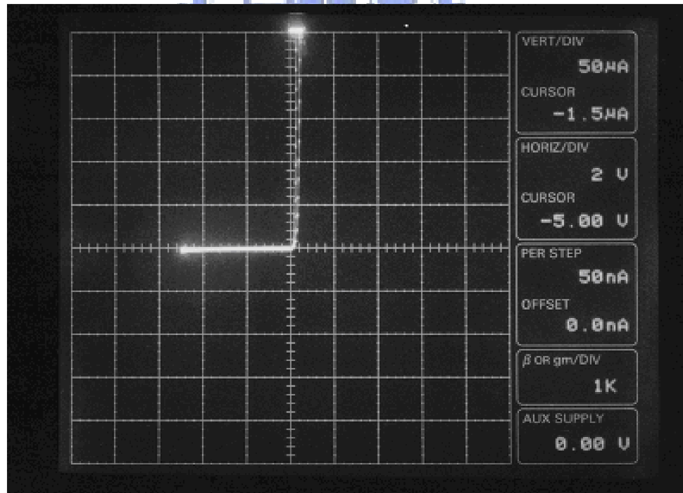

(b)

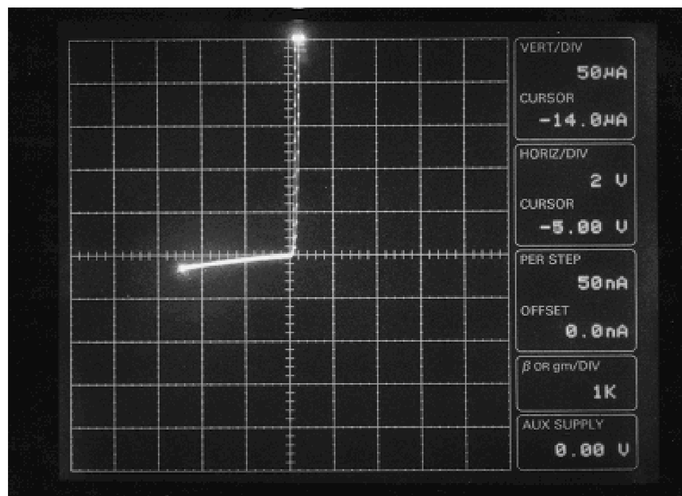

(c)

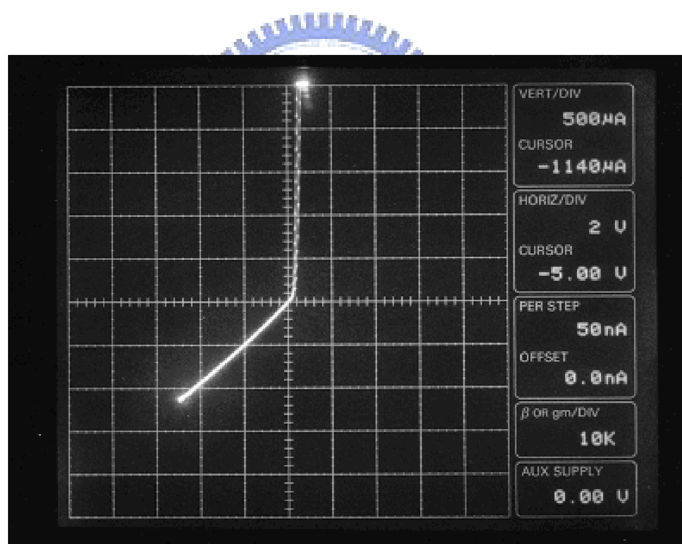

(d)

Figure 2-12(B): Characteristic I–V curves of $Cu/TaN_{1.134}/n^{+}np^{+}$ samples prepared using N_2/Ar as the reactive gas mixture (a) Before thermal treatment and (b–d) after thermal treatment at (b) 500, (c) 550, and (d) 600 °C.

Table 2-1: Highest thermal stability temperatures of $Cu/TaN_X/n^+np^+$ samples.

Reactive gas source	Cu/TaN_X(25nm)/ n^+np^+	The highest thermal stable temperature
NH_3/Ar=0.075	$Cu/TaN_{0.422}$(25nm)/ n^+np^+	450℃
NH_3/Ar=0.175	$Cu/TaN_{0.987}$(25nm)/ n^+np^+	500℃
NH_3/Ar=0.300	$Cu/TaN_{1.277}$(25nm)/ n^+np^+	550℃
N_2/Ar=0.075	$Cu/TaN_{0.313}$(25nm)/ n^+np^+	450℃
N_2/Ar=0.175	$Cu/TaN_{1.134}$(25nm)/ n^+np^+	500℃
N_2/Ar=0.300	$Cu/TaN_{1.418}$(25nm)/ n^+np^+	550℃

Chapter 3

In-Situ Characterization of Cu CMP Slurry and Defect Reduction Using IR Thermal Camera

Abstract

In order to choose appropriate property of Cu CMP (Chemical-Mechanical Polishing) slurry, we used IR thermal camera to distinguish this slurry that belonged to Preston or non-Preston. The adoption of the IR thermal camera is to choose suitable non-Preston Cu CMP slurry in-situ and find out optimal changing timing of step endpoint. Additionally supplementing robust CMP machine, appropriate Cu film quality and pretreatment, we could obtain a total defect number is less than 10^1 order and achieve excellent Cu CMP performance. Such Cu CMP technology resulting in Cu damascene process work and make sure 0.13 μm and beyond 100 nm Cu process to be reliable and practical.

3-1 Introduction

As the line width of ULSI (Ultra-Large Semiconductor Integration) decreases, the problem of RC delay becomes more serious. The replacement aluminum by the copper has been proposed when the line width is smaller than 0.13μm because copper improves conductivity and reduces electro-migration.[1] However, copper has been proven to be not easily etched by plasma. As the Cu CMP process is been developed, the copper damascene process has been made practical.[2] Unfortunately, the properties of copper are such that CMP has produced many defects, including microscratching, dishing, erosion and reduced yield.[3] Hence, this study seeks to develop a new and robust Cu CMP process that can reduce the number of defects and provide a good yield.

Choosing inappropriate slurry would yield a poor Cu CMP performance, including many defects and low yield,[4,5] such that the 0.13 μm Cu process would be ineffective. This experiment utilized an IR thermal camera to select a suitable non-Preston Cu CMP slurry and to diagnose the Cu CMP process in-situ. Adding robust CMP machine and facility, appropriate Cu film quality and pretreatment, yielding an almost perfect Cu CMP process without Cu residues and with a greatly reduced number of defects.

3-2 Experimental Section

This experiment was performed on a Strasbaugh 6ED™ chemical mechanical polisher. Eight-inch wafers of PE-TEOS 7800 Å/ nitride 600 Å /PE-TEOS 5000Å film stack were patterned using a Cu-CMP test mask. A 250 Å TaN, followed by a 700Å Cu seed layer and an 8000μm ECP (Electro-Chemical Plating) Cu film, was deposited by an AMAT cluster tool. A Rodel IC1400 stacked pad and a Non-Preston slurry were used for Cu polishing. During the CMP process, an IR thermal camera captured temperature profile in real time.

3-3 Results and Discussion

The variation in resistivity, the impurity content and the grain size deeply influence the material and electrical properties of a Cu film.[6] Therefore, some proper treatments were applied to the post ECD (Electro-Chemical Deposition) Cu films. Then, the post-CMP results appeared to involve fewer pit defects and microscratches, low resistivity and appropriate grain size. A four-point probe measured the sheet resistances (Rs) of ECD Cu films. Figure 3-1 plots the Rs testing results obtained with treatment at different temperatures. The Rs values of the pre-annealing ECD Cu film were almost the same. After 24 hours of self-annealing, the Cu films were treated for 20 minutes under different conditions - self-annealing, hot plate annealing at 100 ℃, hot plate annealing at 200℃ and furnace annealing at 300℃. The Rs values in Figure 3-1 follow the order self-annealing＞ 100℃ hot plate annealing＞ 300℃ furnace annealing＞ 200℃ hot plate annealing. The Rs value associated with 200℃ hot plate annealing was lower than that associated with 300℃ furnace annealing because the latter case involves a lower vacuum with more impurities, or perhaps incomplete annealing. After 48 hours of self-annealing, the Rs values under all the treatment conditions were almost the same because the Rs values had become stable.

EDS was used to measure the composition and impurity contents of the pre-CMP Cu films, as shown in Figure 3-2, and of the post-CMP Cu films, as shown in Figure 3-3. Increasing the annealing temperature reduced the impure contents. However, for 300℃ furnace annealing, impurity contents were close to those obtained at 100℃ and 200℃ hot plate annealing. Figure 3-2 presents these data. In the experiments, the impure contents were post-Cu CMP. Figure 3-3 shows these results. A Focus Ion Beam (FIB) was used to measure grain sizes of the Cu films; the

sizes were found to increase with annealing temperature, as shown in Figure 3-4.

An IR thermal camera was used to capture the temperature profile of the chips in the Cu CMP process. Figure 3-5a plots the temperature profile associated with slurry A. Several Cu film pre treatments, at 100℃, 200℃ and 300℃, were employed. Increasing the annealing temperature increased the temperature profile obtained using the IR camera. The increase of the temperature profile indicated a stronger CMP reaction and an increased removal rate (RR).[7] While the annealing temperatures increasing, the grain sizes would be grown up (as illustrated in Figure 3-4), and the remove rates (RR) were increased. Slurry A was mechanically dominant (Preston base). For a Cu CMP process with using slurry B, the temperature profile shown in Figure 3-5b was obtained. The highest points of the IR temperature profiles were almost the same at all annealing temperatures. While annealing temperatures increasing, however, the polish times would increase. As the grain boundaries were reduced, the active sites would be decreased, thus resulting in the remove rate was decreased. Slurry B was also determined to be chemically dominant (non-Preston base). In a chemically dominant non-Preston slurry case, the CMP reaction active sites were Cu grain boundaries. The reason was that the Cu CMP mechanism was slurry and Cu form Cu complex compounds then abrasive particles remove the compounds. The active sites were more weak points Cu grain boundaries.

Based on the in-situ IR thermal camera temperature profile, a suitable non-Preston Cu CMP slurry was identified and the Cu CMP process diagnosed. Unlike the Preston slurry that generates many defects, the non-Preston slurry contains a special surfactant that can protect the copper film by forming a complex compound.[8] Thus, the non-Preston slurry is chemically dominant. The use of a Cu film of proper quality, following proper pretreatment, yielded a post CMP total

number of defects of less than 10^1, as measured by a KLA review SEM, as shown as Figure 3-6.

3-4 Conclusions

When the ULSI line width is smaller than 0.13μm, the use of copper is proposed to replace the aluminum. Therefore, a robust Cu CMP technology must be developed to make the Cu damascene process reliable. However, many defects are detrimental to the yield. In this research, an IR thermal camera was used to choose a suitable non-Preston Cu CMP slurry and diagnose the Cu CMP process in real time. Additionally, using a robust CMP machine, a Cu film of appropriate quality, and a suitable pretreatment, enables the Cu CMP process to be greatly improved, with almost no Cu residues or defects.

Reference

[1]. M. T. Bohr, Proceedings of the 1995 IEEE International Electron Device Meeting (1995) 241-242.

[2]. K. H. Holland and etal , “Achieving CMP Manufacturability in the Current Aluminum and Future Copper Damascene Interconnection Technologies”, Semiconductor Fabtech-8th edition (1998) 217.

[3]. Stocckl, P.; Saville, B.; Kavanagh, J.; Dellwig, T. “Advanced cu CMP defect excursion control for leading edge micro-processor manufacturing” Advanced Semiconductor Manufacturing IEEE/SEMI Conference and Workshop (2002) 92 -97.

[4]. P. Wrschka, J. Hernandez et al,Electrochem Soc 147 (2000) 706.

[5]. Wang Xin; Wang Hongying; Liu Yuling, “Development of copper CMP slurry” Solid-State and Integrated-Circuit Technology (2001) 369 –371.

[6]. Alers, G.B.; Dornisch, D.; Siri, J.; Kattige, K.; Tam, L.; Broadbent, E.; Ray, G.W. “Trade-off between reliability and post-CMP defects during recrystallization anneal for copper damascene interconnects” Reliability Physics Symposium, 2001. Proceedings. 39th Annual. 2001 IEEE International (2001) 350 –354.

[7]. H. W. Chiou, and etal , “ On Monitoring CMP Removal Rate by In-Situ Temperature Measurements”, CMP-MIC (2001) 131.

[8]. Alex. Shieh, S. Y. Shih, M. S. Jang, J. X. Lin, Jack. Chen, Y. L. Hwang, C. T. Huang, C. C. Hsueh, Henry. Chung, “Step-by-step characterization in the Cu-CMP by using Non-Preston slurry”, CMP-MIC (2001).

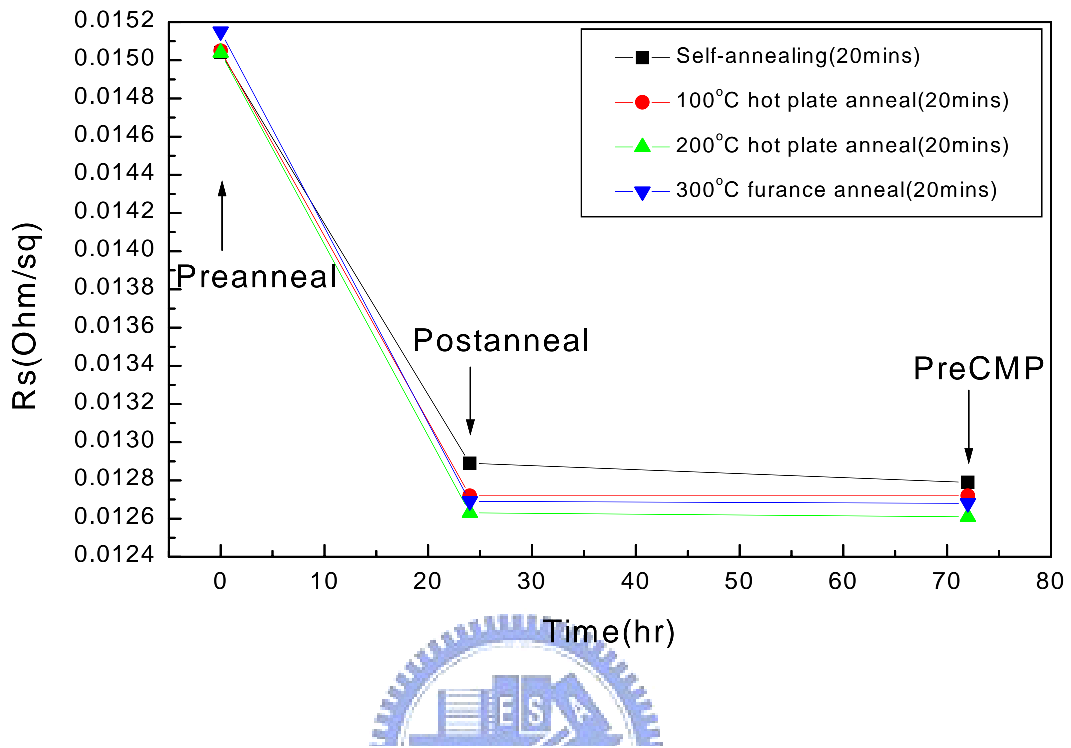

Figure 3-1: Sheet resistance (Rs) testing results with different temperature treatments.

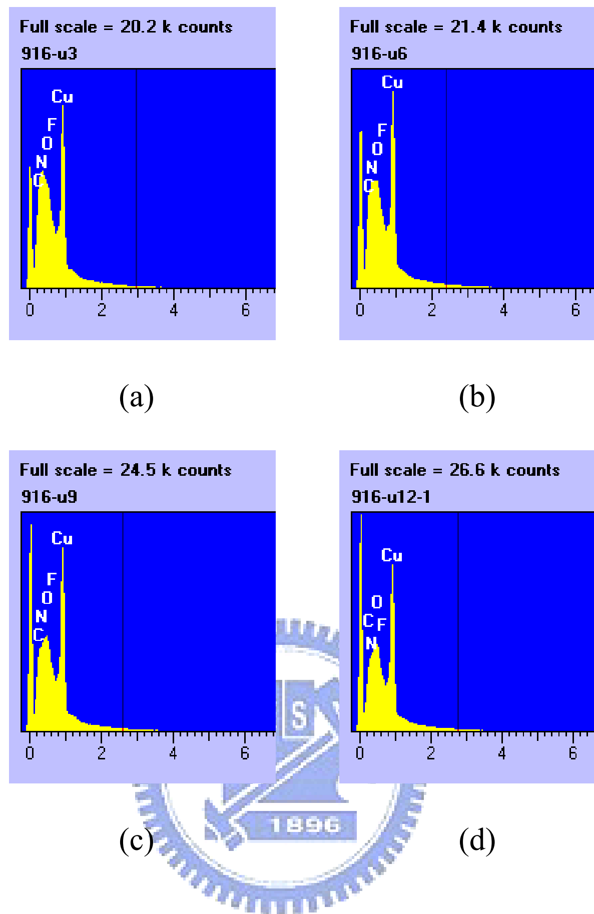

Figure 3-2: EDS measured the components and impurities contain of pre CMP Cu films: (a) self-anneal; (b) 100℃ hot plate annealing; (c) 200℃ hot plate annealing; (d) 300℃ furnace annealing.

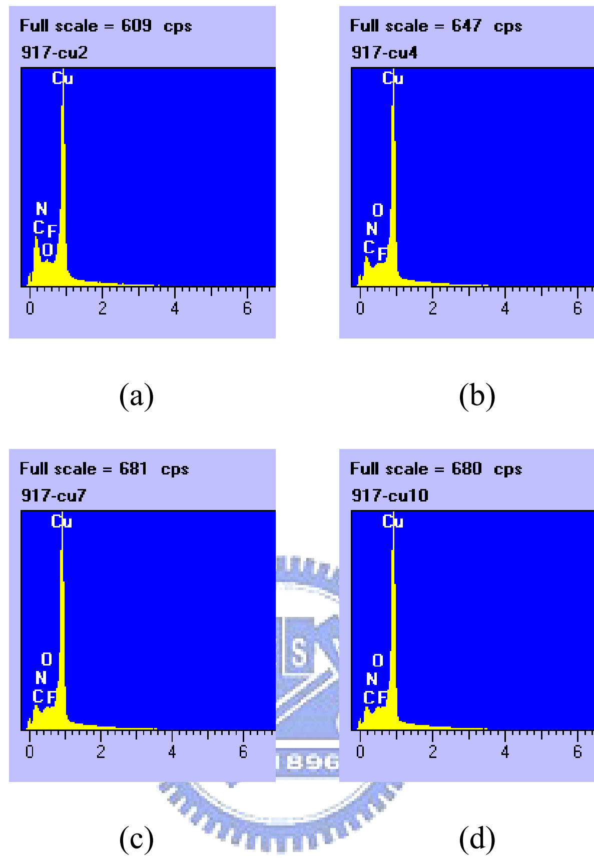

Figure 3-3: EDS measured the components and impurities contain of post CMP Cu films: (a) self-anneal; (b) 100℃ hot plate annealing; (c) 200℃ hot plate annealing; (d) 300℃ furnace annealing.

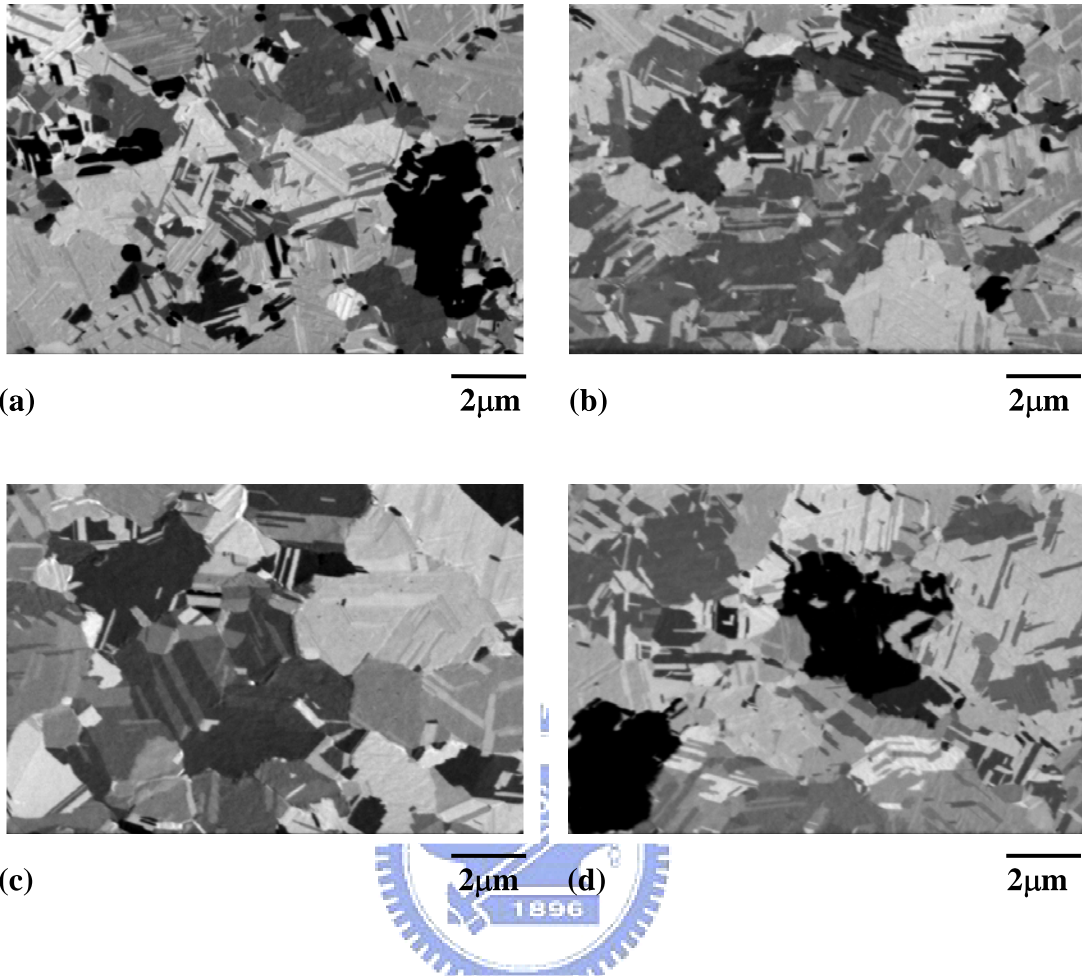

Figure 3-4: Used of FIB to measure post annealing Cu films grain sizes: (a) self-anneal; (b) 100℃ hot plate annealing; (c) 200℃ hot plate annealing; (d) 300℃ furnace annealing.

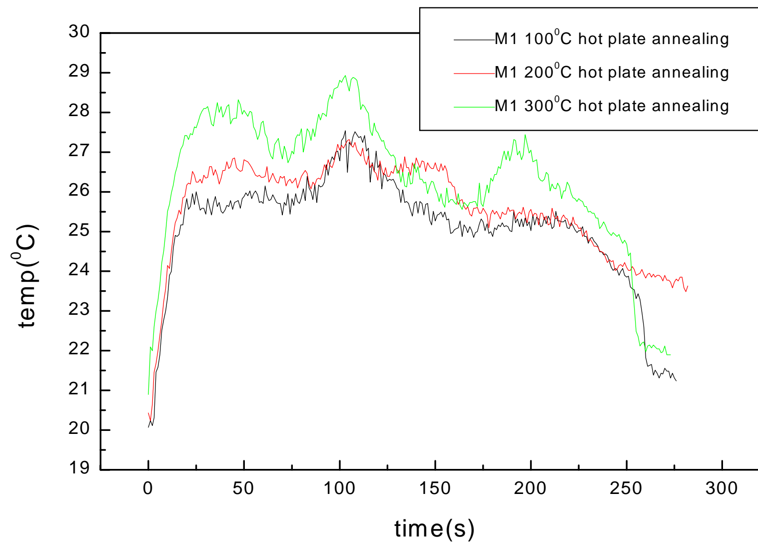

(a)

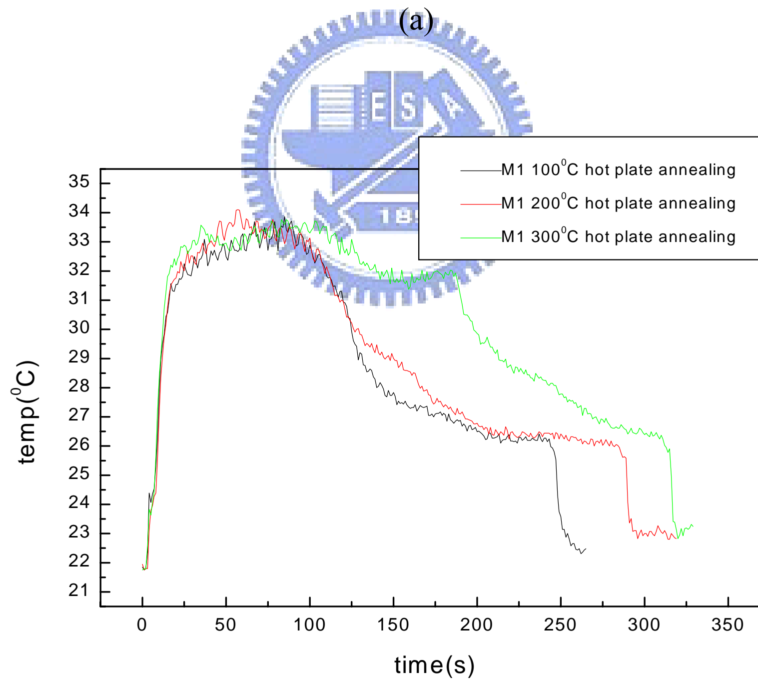

(b)

Figure 3-5: Used of IR thermal camera to catch Cu CMP process temperature profile: (a) the temperature profile of Cu CMP process with slurry A mechanical dominant slurry (Preston base); (b) the temperature profile of Cu CMP process with slurry B chemical dominant slurry (non-Preston base).

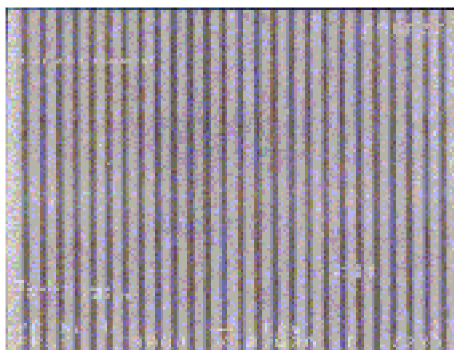

1μm

Figure 3-6: Used of KLA review SEM to see post Cu CMP process defect results.

Chapter 4

Immobilization of DNA Extraction Beads in Polymeric Microfluidic Biochip for Sample-Preparation

Abstract

"Lab-on-a-chip (LOC)" is a name for devices that integrate multiple laboratory functions on a single chip with an area of only millimeters to a few square centimeters. Such chips can handle extremely small fluid volumes down to less than pico liters. The sample-preparation procedure and the experimental steps for automating sample-preparation are important design considerations. In this study, DNA extraction beads were fixed on the sample-preparation chip to improve the following four factors - acceleration of sample-preparation procedure, minimization of required sample quantity, simplification of sample-preparation and complete automation of the process.

When DNA extraction beads were not fixed on the sample-preparation chip, simply mixing them with biochemical solution caused the macromolecule hinder the combination of DNA with the functional base group, even when the liquid flows back-and-forth. When DNA extraction beads were fixed on the sample-preparation chip, the collision rate of both reactants increased that increasing the extraction efficiency. A thin micro layer of polymer solution could fix the DNA extraction beads on the substrate surface, but plasma treatment of the chip substrate altered and activated its surface. Hence, the DNA extraction beads could bond covalently with the substrate surface, further improving the efficiency of DNA extraction.

4-1 Introduction

Biochips have potential applications in the fundamental research in life sciences, the development of new drugs, clinical disease diagnosis, food security and the chemical industry, among other areas.[1-8] Among commercialized biochips, DNA chips that contain thousands of microscopic DNA probes per unit area have been well developed and effective. They can be used to analyze the expression of multiple genes simultaneously. Conventional analysis of gene expression uses many instruments for the preparation, amplification and final detection of sample. However, biotechnical micro electro mechanical systems (BioMEMS) replace large biochemical instruments with a small LOC which facilitates a complete set of successive biochemical experiment steps on a microchip and integrates multiply functions automated laboratory.[9] LOC is fully/highly automated, lightweight, easy to use, low cost, short test cycle time and reduce the need for samples.

The complexity of blood samples requires tedious procedures to extract, separate, condense and amplify the desired DNA. A sample-preparation chip has been developed by using DNA extraction beads fixing on microfluidic channels to accelerate the preparation of the sample and to overcome the aforementioned difficulties. Fixing DNA extraction beads on the chip reduces the amount of sample required, simplifying and fully automating the procedure.

In this study, DNA extraction beads are fixed on the substrate surface by chemical solution or plasma treatment. The DNA extraction beads can be covalently bonded with the substrate surface by altering and activating the substrate surface. The DNA extraction beads are fixed on the chip, and then create a microfluid moving back-and-forth. Microfluidic convection further increases the effective collision between DNA and beads, improving the efficiency of DNA extraction.

4-2 Experimental Section

PMMA and PC are used as substrate materials because they can be easily processed and disposable.[10-11] The polymer was dissolved in a proper solvent to form a homogeneous solution such as PMMA/EA-MeOH or PMMA/THF-MeOH.[12] The solution of 5.0 wt% DNA extraction beads was spin-coated on the substrate to yield a uniform coating of DNA extraction beads. After heating at 80 °C for 30 min, these beads could easily bind to the surface covalently. 75 volume% NH_3 + 25 volume% O_2 plasma treatment on the PMMA polymer substrate surface for 3 min was also performed to increase its chemical activity. The RF power was fixed at 300 W, base pressure was 5×10^{-7} torr, NH_3 gas flow rate was 6 SCCM and O_2 gas flow rate was 2 SCCM and the operating pressure was 3×10^{-2} torr. The plasma treated PMMA substrate was then coated evenly with an aqueous solution containing 5.0 wt% DNA extraction beads. After heating at 80 °C for 30 min, these beads bonded easily and covalently to the substrate surface. The solution of DNA was added to the sample-preparation chip to extract the DNA using air pump to control moving back-and-forth. Processes flowing were: 100 ng *Escherichia coli (E. coli)* cells (10^2 μl^{-1}) with 200 μl whole blood + 100 μl buffer solution (B1+B2, Magic Bead, USA) in beads channel to lyse the cells and to extract *E. coli* genomic DNA at room temperature for 5 min → 100 μl buffer solution to wash beads channel at room temperature for 5 min → 50 μl d.d H_2O to elution DNA. After the extraction, the polymerase-chain-reaction (PCR) and agarose gel electrophoresis were performed for qualitative analysis (to separate DNA strands by size). PCR forward and reverse primers used were 5A-CAGGATTAGATACCCTGGTAG-3A and 5ATTCCCCTACGGTTACCTTGTT-3A, respectively, and the length of the PCR product was 620 bp; PCR (PCR system MJ PTC-100) processes conditions were one

cycle of 5 min at 95 °C, 40 cycles of 30 s at 95 °C, 40 s at 58 °C and 40 s at 72 °C, and one cycle of 10 min at 72 °C. PCR products corresponded to the amplified 16S rRNA in the DNA fragments of *E. coli* genomic DNA. DNA ladders (SM0633, Taiwan Flow, Taiwan; DM100-2, Bioman, Taiwan) were used as markers in the gel electrophoresis. Finally, quantitative experiments with an Agilent 2100 bioanalyzer (Agilent Technologies, USA) were carried out.

4-3 Results and Discussion

Several methods of biochemical sample-preparation are currently available, only well-trained biochemists can perform these complicated DNA extraction procedures. The processes flowing are shown in Figure 4-1: Adding phenol, chloroform and isoamyl alcohol + bio samples (including DNA, RNA, proteins, etc.) then centrifuge → Transfer liquid to get DNA solution and adding sodium acetate/100 % ethanol then centrifuge → Repeating discard liquid and adding 70 % Ethanol until to get pure solid DNA. Auxiliary biochemical reagents or apparatus have been developed for general operators, however, these reagents and apparatus are expensive and the procedures are still complicated. The traditional bead method of DNA extraction is also complicated and time-consuming. The processes flowing are shown in Figure 4-2: Adding NaI, glass beads + bio samples (including DNA, RNA, proteins, etc.) then incubate at room temp for 5 min to let beads adsorption DNA → Centrifuge then discard liquid washing 3 times to get pure beads adsorption DNA → Incubate at 45 °C for 3 min then adding TE buffer to let DNA adsorption from beads → Centrifuge then transfer liquid to get pure DNA in TE buffer. For these reasons, a chip that integrating these processes was developed to increase the accuracy and accelerate the preparation of the sample, while reducing the cost. Figure 4-3(a) showed the DNA extraction chip consisting of microfluidic channels (Figure 4-3(b)) and samples injection channels (Figure 4-3(c)). The DNA extraction beads were coated on the microfluidic channels (Figure 4-3(b)) and bonded covalently to the channel surface. Samples were injected into the microfluidic channel through the injection channel (Figure 4-3(c)). The processes flowing were: Bio samples (including DNA, RNA, proteins, etc.) + 100 μl buffer solution (B1+B2, Magic Bead, USA) in beads channel to lyse the cells and to extract DNA at room temperature for 5 min → 100 μl buffer

solution to wash beads channel at room temperature for 5 min → 50 μl d.d H_2O to elution DNA. The "immobilization of DNA extraction beads" and "back-and-forth microfluidic flow" were both important in designing this novel DNA extraction chip because they could increase the efficiency of DNA extraction by increasing the probability of collision between both reactants.[13-15] DNA extraction beads could only mix in the sample solution but did not bond covalently on the surface of the microfluidic channel. However, the present of impurities tended to reduce the opportunity of a reaction between DNA and the beads even under back-and-forth microfluidic flow conditions as shown in Figure 4-4(a). Figure 4-4(b) showed the condition under which the DNA extraction beads were bonded covalently on the microfluidic channels to increase the collision rate between DNA and beads, and thus improved the extraction efficiency. Table 1 compares relative performances from these three sample preparation procedures for the DNA extraction technology.

Quartz has been used extensively as a substrate material of chips because Si-OH groups on the surface can promote the chemical reaction in the microfluidic channels on the chip.[16] However, quartz is expensive and the process is time-consuming. For substitution, a transparent polymer material PMMA was chosen for the biochip substrate. PMMA is lightweight, low cost and easy to process. Its refractive index is similar to that of optical glass and is called "optical plastic". Meanwhile, PC exhibits excellent shock-resistance, high rigidity, high tensile/flexural strength, high heat deflection temperature, excellent transparency, low mold shrinkage and high biological compatibility. Given these advantages, PMMA and PC were used herein as substrate materials in our designed chip.

Since the surface of the polymer film is neutral, it exhibits low adsorption of the sample and low reactivity between the bio-molecules and the substrate surface.

Bio-molecules can be attached to the substrate by hydrophobic interaction or the Van der Waals force. These unstable interactions cause desorption easily and consequently decrease in yield. In this experiment, the PMMA and PC substrates were coated with a thin micro layer of PMMA polymer solution of specific concentration. The -C=O functional group in the thin polymer layer interacted with the -NH group in the DNA extraction beads to form the –CONH amide covalent bond,[17] which provided a stable and strong bonding force to fix the DNA extraction beads robustly on the substrate surface. Later, the DNA solution was then added to extract DNA and amplified the DNA by PCR. The extraction was analyzed by using agarose gel electrophoresis. PMMA substrate was also treated with NH_3 + O_2 plasma to change its surface state and to activate -C=O bonds on the PMMA substrate. The activated -C=O groups were able to react with the -NH groups of the DNA extraction beads to form –CONH amide covalent bonds to proceed the DNA extraction and post-PCR biochemical testing.

Qualitative analyses were performed to characterize substrate surface reactions after treating with different solutions. Different solvents and polymer solutions caused different chemical reactions on the substrate surface. Therefore, appropriate solution must be chosen with proper solubility to dissolve PMMA without damaging the surface of the substrate and to form a thin film on the substrate. Different substrates against different solutions were carried out. Using ethyl acetate (EA), toluene, acetone and chloroform solutions to treat PMMA substrates did not damage the substrates surfaces. The least toxic and less volatile solvent, ethyl acetate (EA), was chosen to treat the PMMA surface. The polymer was dissolved in EA solvent, methanol (MeOH) was then added to yield homogenous solution, and then spin coating was carried out to coat the solution uniformly on the substrate. The spin

frequency, time and solution viscosity were chosen according to the required thickness and uniformity of the film. The following experimental steps were repeated, and the spin-coating steps conducted to coat uniformly the solution on the substrate were: 700 rpm × 30 sec → 1500 rpm × 10 sec → 2500 rpm × 10 sec → 1000 rpm × 20 sec for solutions with 5.0 wt% DNA extraction beads and concentrations of 5.0 wt%, 10.0 wt%, 15.0 wt% and 20.0 wt% PMMA/EA-MeOH of the PMMA substrate. After heating at 80 °C for 30 min, the residues unabling to be fixed on the substrate surface were cleaned off. The dispersion of DNA extraction beads fixed on the substrate surface was treated with different solutions of various concentrations. The distribution of these beads on the surface was then investigated and used as a benchmark for modifying the solution formula. The optical microscope images obtained in this experiment were shown in Figure 4-5.

Figure 4-5 showed that the uniformity of the DNA extraction beads dispersion decreased as the concentration of PMMA/EA-MeOH was increased. When the solution concentration was too low at 5.0 wt% PMMA/EA-MeOH, these DNA extraction beads were dispersed uniformly (Figure 4-5(a)). However, these beads did not fix well on the substrate that could be peeled off easily after cleaning and result in reduced yield. DNA extraction and PCR were carried out on a DNA containing solution, followed by agarose gel electrophoresis. The processes flowing were the same section 2 experimental mention. Results of DNA extraction were shown in Figure 4-6, where lanes (1) ~ (2) were positive control, lane (3) was 5.0 wt% PMMA/EA-MeOH, lane (4) was 10.0 wt% PMMA/EA-MeOH, lane (5) was 15.0 wt% PMMA/EA-MeOH and lane (6) was 20.0 wt% PMMA/EA-MeOH. In Figure 4-6 lane (3) showed that the brightness of the agarose gel electrophoresis diagram of the 5.0 wt% PMMA/EA-MeOH was lower than that of other lanes. If the solution

concentration is too high at 20.0 wt% PMMA/EA-MeOH, these beads were easily aggregated and covered by the polymer thin layer; therefore, the beads active sites would decrease as shown in Figure 4-5(d). In Figure 4-6 lane (6), the brightness of the agarose gel electrophoresis diagram was lower than that in Figure 4-6 lanes (5). Different intermolecular interactions affect the solution phase behavior. When the polymer was highly soluble in the selected solvent, the phase segregation disappears and the thin-film formed from such polymer solution is more uniform.

A polycarbonate (PC) was also chosen for the biochip substrate and qualitative analyses were performed to characterize substrate surface reactions after treating with different solutions. Using MeOH, EA, tetrahydrofuran (THF) and toluene solutions to treat PC substrates did damage the substrates surfaces. The least toxic and less volatile solvent, MeOH, was chosen to treat the PC surface. The solubility of the polymer in the MeOH solution was relatively low; THF buffer solution was added to improve its solubility. Spin coating was then carried out to coat the solution uniformly on the substrate. The optical microscope images obtained in this experiment were shown in Figure 4-7.

Figure 4-7 showed that the uniformity of the DNA extraction beads dispersion decreased as the concentration of PMMA/THF-MeOH was increased. DNA extraction and PCR were carried out on a DNA containing solution, followed by agarose gel electrophoresis. The processes flowing were the same section 2 experimental mention. Results of DNA extraction were shown in Figure 4-8. Figure 4-8 lane (1) was 5.0 wt% PMMA/THF-MeOH, lane (2) was 10.0 wt% PMMA/THF-MeOH, lane (3) was 15.0 wt% PMMA/THF-MeOH and Lane (6) was positive control. If the solution concentration was too high at 20.0 wt% PMMA/

THF-MeOH, these beads were easily aggregated and covered by the polymer thin layer, the number of beads active sites would decrease as shown in Figure 4-7(d).

Base on above results, PMMA was a more suitable substrate material than PC. The agarose gel electrophoresis diagrams of these two different substrates agreed with the experimental results (Figure 4-6 and Figure 4-8). The brightness in the agarose gel electrophoresis diagram of Figure 4-8 was lower and more diverse than Figure 4-6. Therefore, PMMA was chosen as the substrate material and treated with NH_3 + O_2 plasma to activate surface. Then the substrate surface was coated with an aqueous solution of 5.0 wt% DNA extraction beads and uniform heating at 80 °C for 30 min was applied to activate the DNA extraction beads to promote covalent bonding with the polymer substrate surface. Figure 4-9 showed the agarose gel electrophoresis diagram of fixed DNA extraction beads under NH_3 + O_2 plasma treatment and free beads. The brightness of the agarose gel electrophoresis diagrams associated with the used of DNA extraction beads inside the sample-preparation chip (lane (5)) exceeded that obtained by using free beads (lane (2)). The used of DNA extraction beads in the sample-preparation chip to extract DNA were more efficient than the used of free beads. These samples were further analyzed using an Agilent 2100 bioanalyzer as shown in Figure 4-10. When DNA extraction beads inside a sample preparation chip were used to extract DNA, the DNA concentration of 0.25 ng μl^{-1} was obtained higher than that obtained by using free beads at 0.16 ng μl^{-1}.

4-4 Conclusions

The PMMA is chosen as the biochip substrate. The PMMA polymer solution is applied to treat the substrate surface to fix the DNA extraction beads, this approach provides an attractive intermolecular force between DNA and the substrate surface by the DNA extraction method base on results from PCR amplification and agarose gel electrophoresis testing. The brightness in the agarose gel electrophoresis test indicates that as the electrophoresis diagrams have higher brightness, more DNA is attached in the test. A polymer solution can fix the DNA extraction beads on the substrate surface. In addition, plasma treatment on the substrate activates the surface and thus promotes covalent bonding of DNA extraction beads with the substrate surface and improves extraction efficiency. This study provides a practical and efficient method for LOC to be more realistic.

References

[1] Francia, Girolamo Di, Ferrara, Vera La, Manzo, Sonia, Chiavarini, Salvatore, Towards a label-free optical porous silicon DNA sensor. Biosensors and Bioelectronics, 21(2005) 661-665.

[2] Liu, Wen-Tso, Zhu, Liang, Environmental microbiology-on-a-chip and its future impacts. Trends in Biotechnology, 23 (2005) 174-179.

[3] Wang, Chih-Hao, Lee, Gwo-Bin, Automatic bio-sampling chips integrated with micro-pumps and micro-valves for disease detection. Biosensors and Bioelectronics, 21 (2005) 419-425.

[4] Di Francia, G., Castaldo, A., Massera, E., Nasti, I., Quercia, L., Rea, I., A very sensitive porous silicon based humidity sensor. Sensors & Actuators: B. 111 (2005) 135-139.

[5] Campàs, M., Katakis, I., DNA biochip arraying, detection and amplification strategies. Trends in Analytical Chemistry, 23 (2004) 49-62.

[6] Cheng, Yi-Ting, Pun, Ching-Chin, Tsai, Chien-Ying, Chen, Ping-Hei, An array-based CMOS biochip for electrical detection of DNA with multilayer self-assembly gold nanoparticles. Sensors & Actuators: B. 109 (2005) 249-255.

[7] Antje J. Baeumner, Richard N. Cohen, Vonya Miksic, Junhong Min, RNA biosensor for the rapid detection of viable Escherichia coli in drinking water. Biosensors and Bioelectronics, 18 (2003) 405-413.

[8] Wenting Zhao, Shanjing Yao, I.-Ming Hsing, A microsystem compatible strategy for viable *Escherichia coli* detection. Biosensors and Bioelectronics, 21 (2006) 1163-1170.

[9] Masaki Yamaguchi, Shigenori Kambe, Takashi Eto, Masaru Yamakoshi, Takuji Kouzuma, Nobuyuki Suzuki, Biosensors and Bioelectronics, 21 (2005) 426-432.

[10] M. Jeong, Mackay, M. E., Intrinsic Viscosity Variation in Different Solvents for Dendrimers and Their Hybrid Copolymers with Linear Polymers. Macromolecules, 34 (2001) 4927-4936.

[11] Siriwan Suwansa-ard, Proespichaya Kanatharana, Punnee Asawatreratanakul, Chusak Limsakul, Booncharoen Wongkittisuksa, Panote Thavarungkul, Semi disposable reactor biosensors for detecting carbamate pesticides in water. Biosensors and Bioelectronics, 21 (2005) 445-454.

[12] Nishiyama, N., Tanaka, S., Egashira, Y., Oku, Y., Ueyama, K., Enhancement of Structural Stability of Mesoporous Silica Thin Films Prepared by Spin-Coating. Chem, Mater, 14 (2002) 4229.

[13] Siu Wai Yeung, I-Ming Hsing, Manipulation and extraction of genomic DNA from cell lysate by functionalized magnetic particles for lab on a chip applications. Biosensors and Bioelectronics, 21 (2006) 989-997.

[14] Xiangling Ren, Xianwei Meng, Dong Chen, Fangqiong Tang, Jun Jiao, Using silver nanoparticle to enhance current response of biosensor. Biosensors and Bioelectronics, 21 (2005) 433-437.

[15] Zhiai Xu, Zhihui Guo, Shaojun Dong, Electrogenerated chemiluminescence biosensor with alcohol dehydrogenase and tris(2,2_-bipyridyl)ruthenium (II) immobilized in sol–gel hybrid material. Biosensors and Bioelectronics, 21 (2005) 455-461.

[16] Todd Strother, Robert J. Hamers, Lloyd M. Smith, Covalent attachment of oligodeoxyribonucleotides to amine-modified Si (001) surfaces. Nucleic Acids Res. 18 (2000) 3535-3541.

[17] C. H. Lin, The research of molecular link on the surface of biochip. NCTU, master paper. 2004.

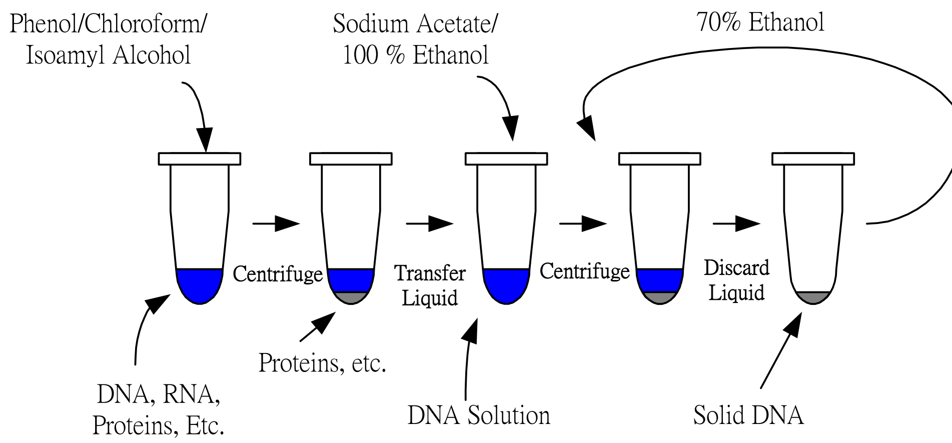

Figure 4-1: Process flow chart of human method for DNA extraction.

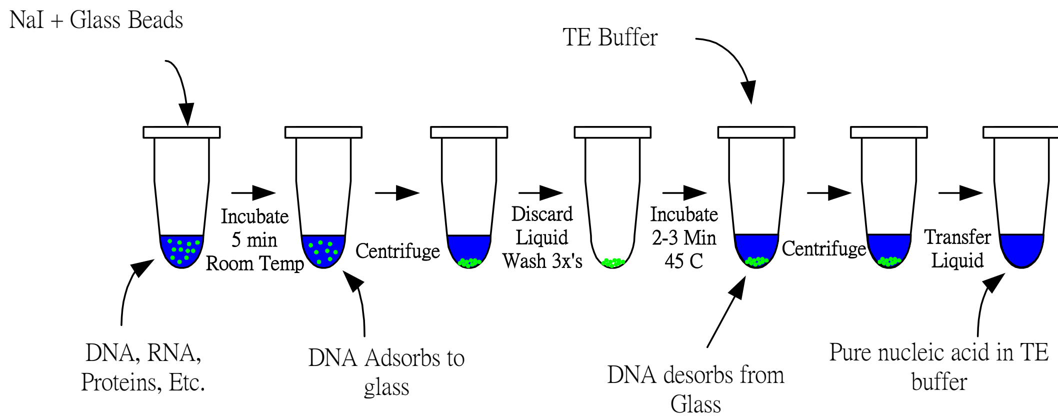

Figure 4-2: Process flow chart of tradition beads method for DNA extraction.

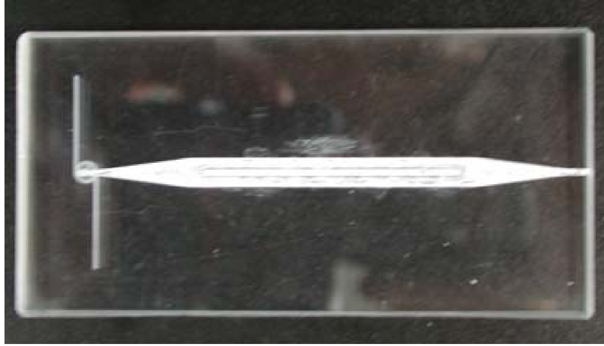

Figure 4-3: (a) Photo image of the DNA extraction sample-preparation chip with DNA extraction beads fixed on.

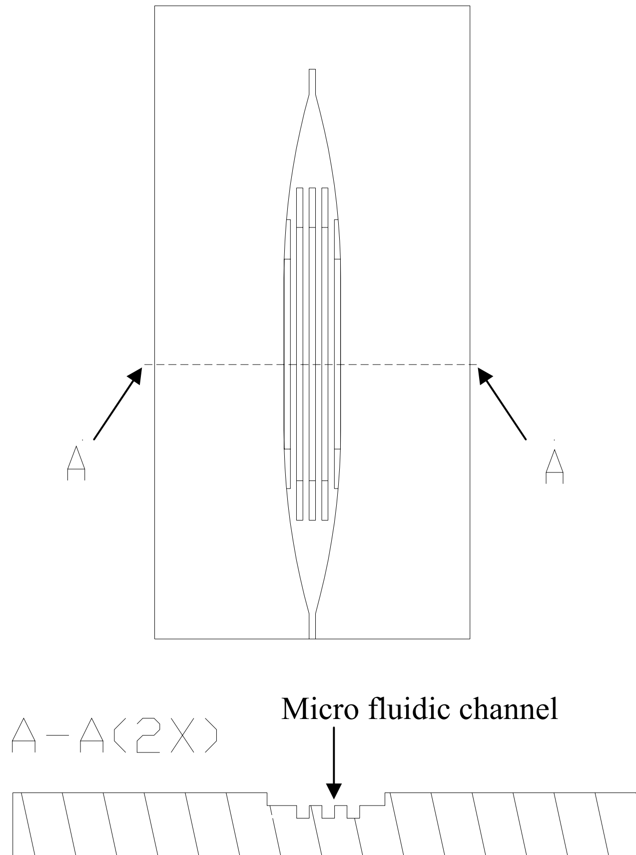

Figure 4-3: (b) Schematic drawing of the microfluidic channels of sample-preparation chip for DNA extraction beads fixed on.

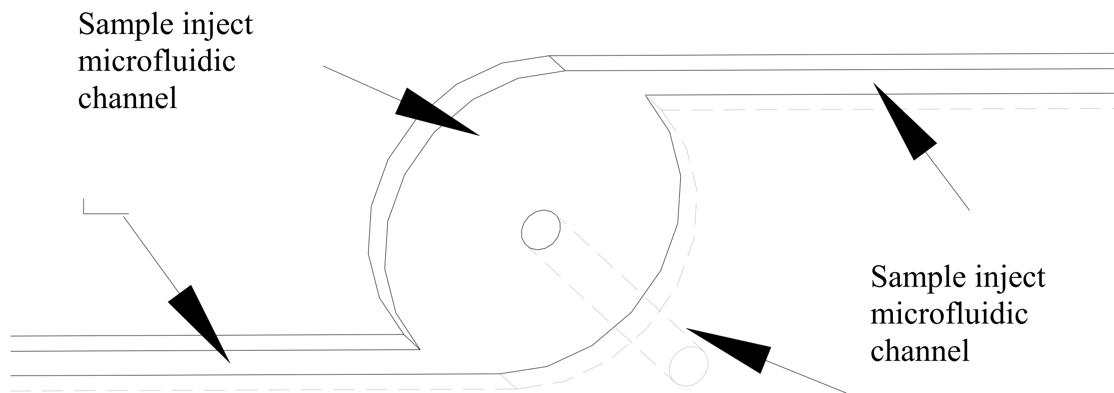

Figure 4-3: (c) Schematic drawing of the microfluidic channels of sample-preparation chip for injected of DNA solution samples in.

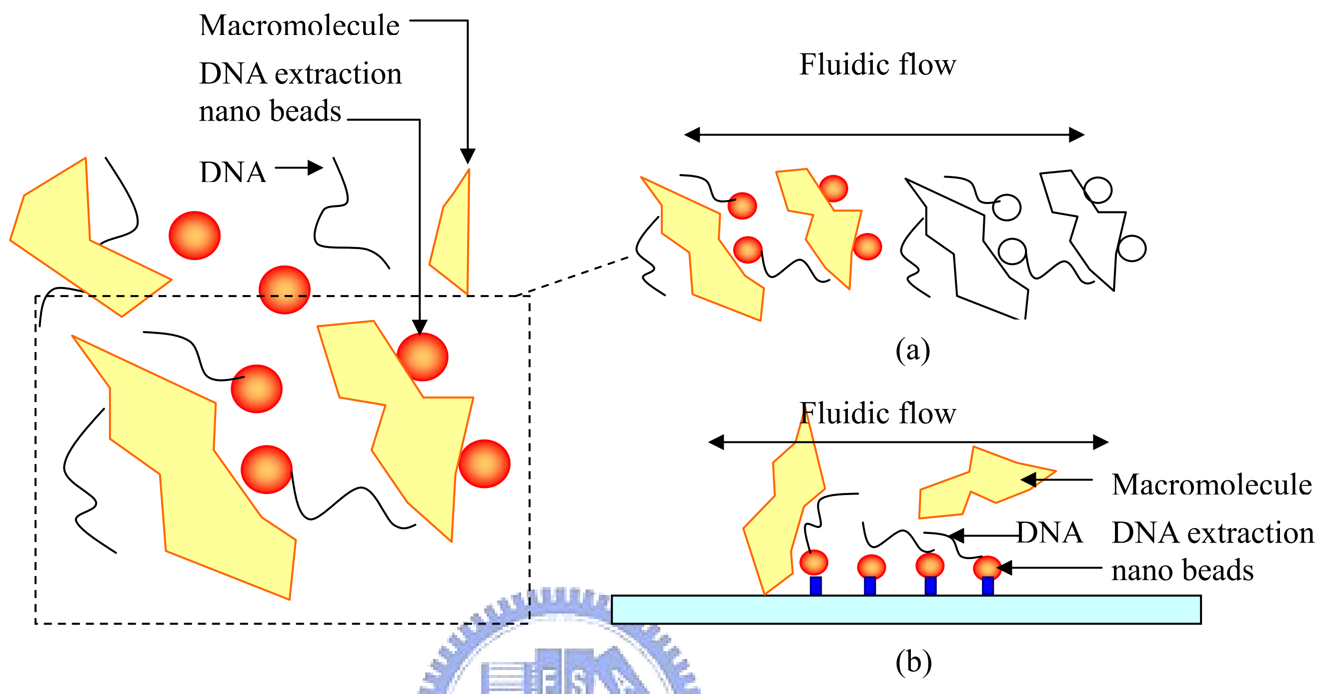

Figure 4-4: (a) DNA extraction mechanism without fixed DNA extraction beads on microfluidic channels. (b) DNA extraction mechanism with fixed DNA extraction beads on microfluidic channels.

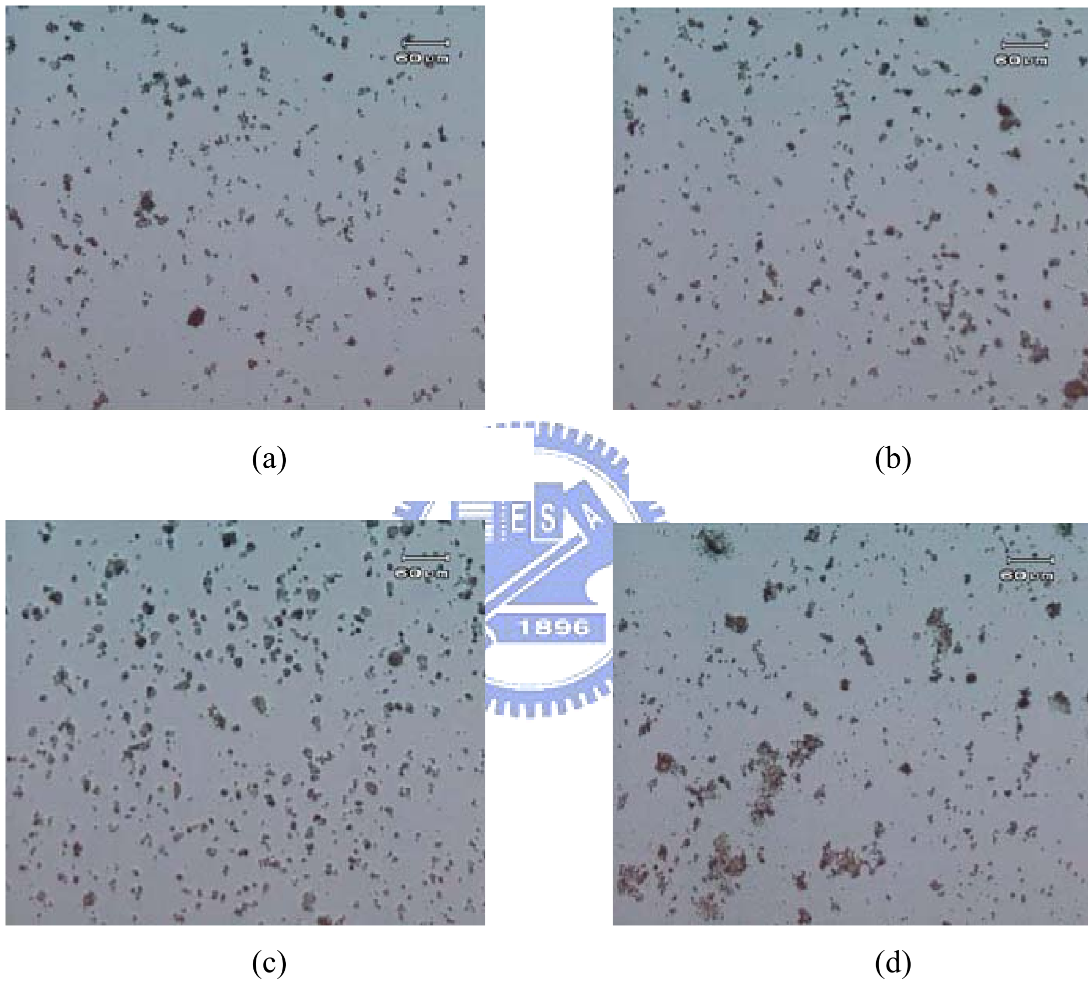

Figure 4-5: Optical microscope images – Dispersing solutions of different concentration on PMMA substrates (a) 5.0 wt% PMMA/EA-MeOH, (b) 10.0 wt% PMMA/EA-MeOH, (c) 15.0 wt% PMMA/EA-MeOH, (d) 20.0 wt% PMMA/EA-MeOH.

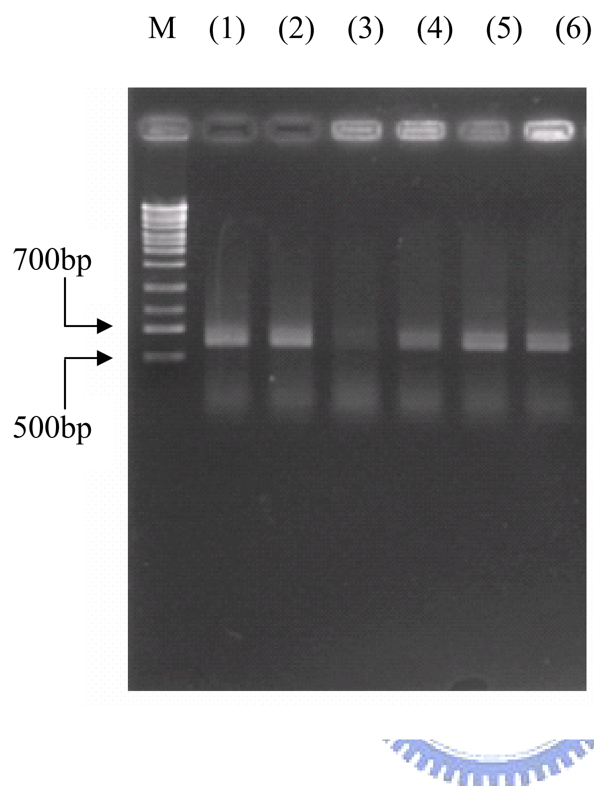

Figure 4-6: Agarose gel electrophoresis diagram of DNA extraction beads inside sample preparation chip with different concentration PMMA/EA-MeOH on PMMA substrate. Lane (1) ~ (2) were positive control; Lane (3) was 5.0 wt% PMMA/EA-MeOH; Lane (4) was 10.0 wt% PMMA/EA-MeOH; Lane (5) was 15.0 wt% PMMA/EA-MeOH; Lane (6) was 20.0 wt% PMMA/EA-MeOH.

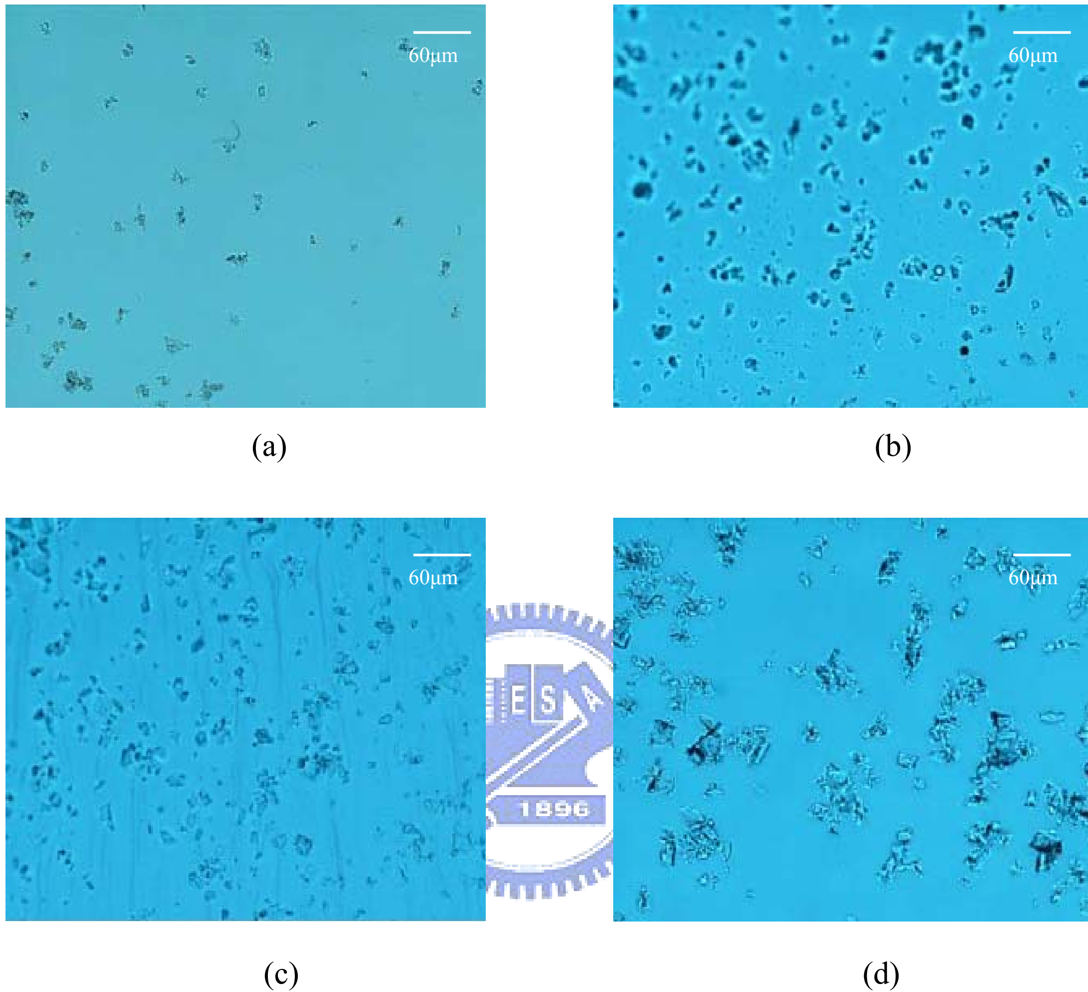

Figure 4-7: Optical microscope images – Dispersing solutions of different concentration on PC substrates (a) 5.0 wt% PMMA/THF-MeOH, (b) 10.0 wt% PMMA/THF-MeOH, (c) 15.0 wt% PMMA/THF-MeOH, (d) 20.0 wt% PMMA/THF-MeOH.

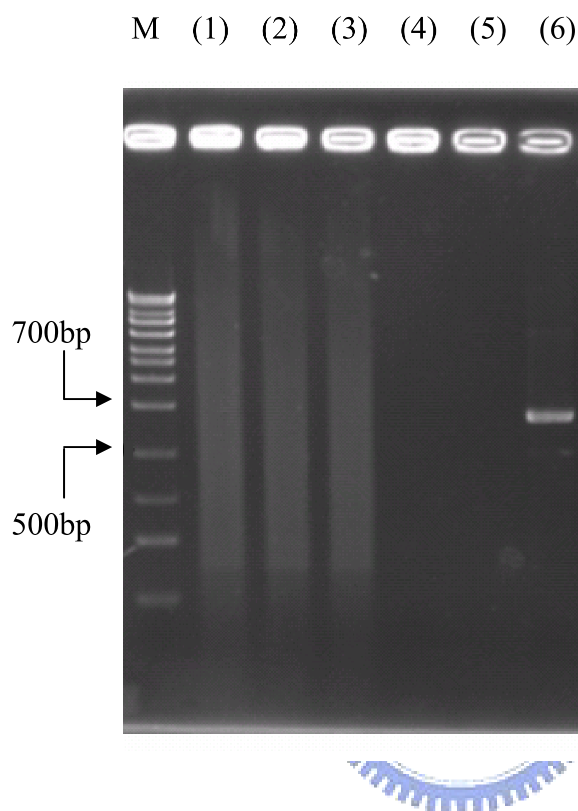

Figure 4-8: Agarose gel electrophoresis diagram of DNA extraction beads inside sample-preparation chip with different concentration PMMA/THF-MeOH on PC substrate. Lane (1) was 5.0 wt% PMMA/THF-MeOH; Lane (2) was 10.0 wt% PMMA/THF-MeOH; Lane (3) was 15.0 wt% PMMA/THF-MeOH; Lane (6) was positive control.

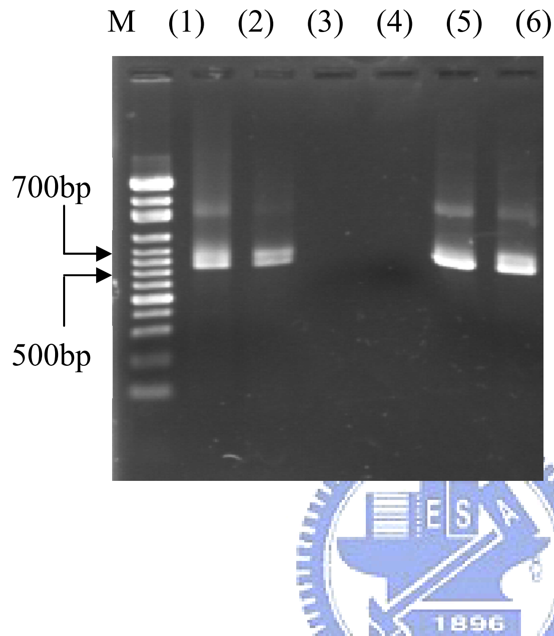

Figure 4-9: Comparison of agarose gel electrophoresis diagram of fixed DNA extraction beads under NH_3 + O_2 plasma surface treatment and free beads. Lane (1) was free beads (50 ng *E. coli* cells), Lane (2) was free beads (100 ng *E. coli* cells), Lane (3) was beads inside sample-preparation chip pre using wash, Lane (4) was collecting beads inside sample-preparation chip wash, Lane (5) was beads inside sample-preparation chip elution (100 ng *E. coli* cells), Lane (6) was positive control.

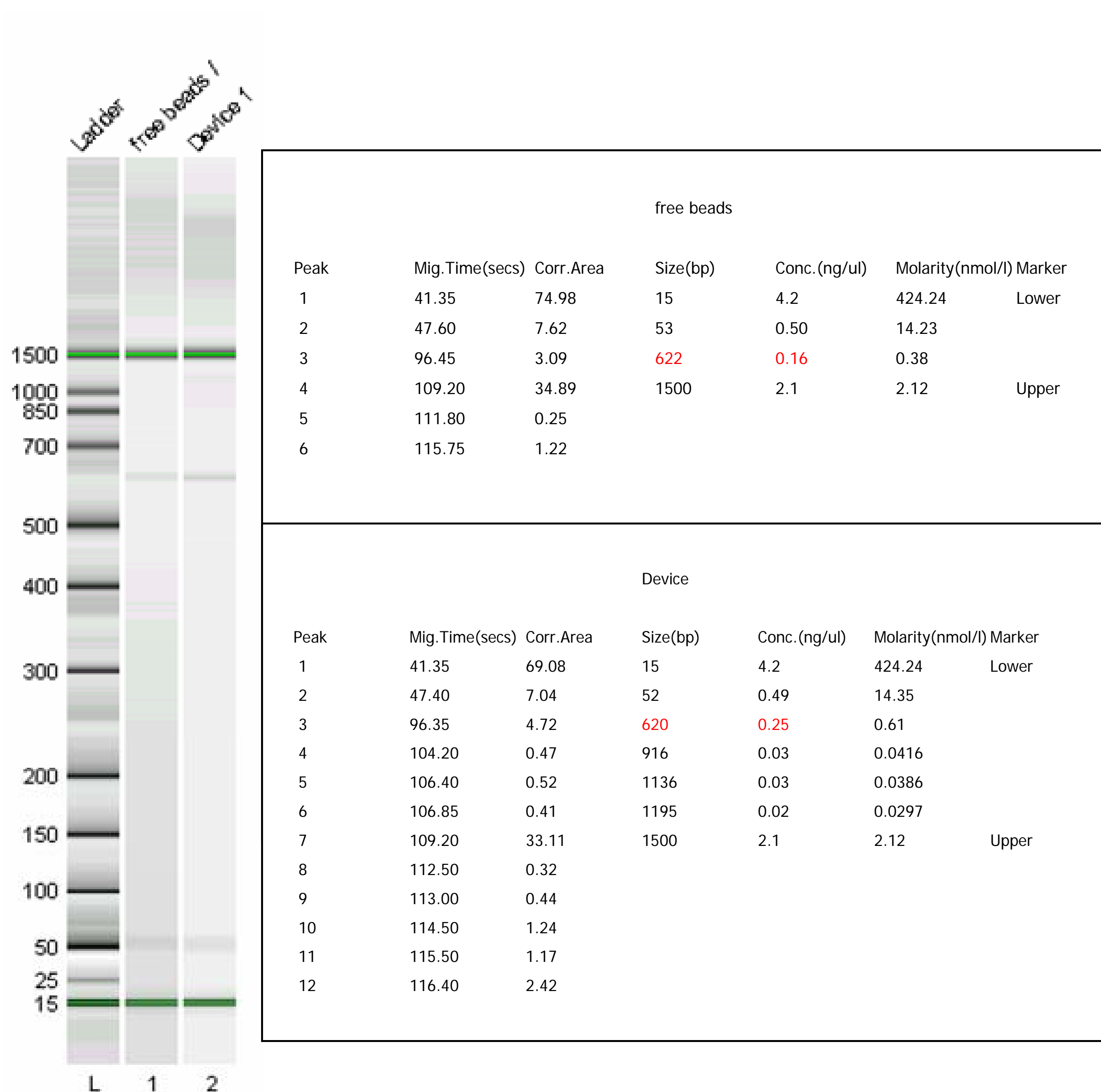

free beads

Peak	Mig.Time(secs)	Corr.Area	Size(bp)	Conc.(ng/ul)	Molarity(nmol/l)	Marker
1	41.35	74.98	15	4.2	424.24	Lower
2	47.60	7.62	53	0.50	14.23	
3	96.45	3.09	622	0.16	0.38	
4	109.20	34.89	1500	2.1	2.12	Upper
5	111.80	0.25				
6	115.75	1.22				

Device

Peak	Mig.Time(secs)	Corr.Area	Size(bp)	Conc.(ng/ul)	Molarity(nmol/l)	Marker
1	41.35	69.08	15	4.2	424.24	Lower
2	47.40	7.04	52	0.49	14.35	
3	96.35	4.72	620	0.25	0.61	
4	104.20	0.47	916	0.03	0.0416	
5	106.40	0.52	1136	0.03	0.0386	
6	106.85	0.41	1195	0.02	0.0297	
7	109.20	33.11	1500	2.1	2.12	Upper
8	112.50	0.32				
9	113.00	0.44				
10	114.50	1.24				
11	115.50	1.17				
12	116.40	2.42				

Figure 4-10: Comparison of Agilent 2100 bioanalyzer analysis diagram and data of fixed on DNA extraction beads (100 ng *E. coli* cells) under NH_3 + O_2 plasma surface treatment and free beads (100 ng *E. coli* cells).

Table 4-1: Comparison of three sample preparation methods for DNA extraction.

Comparing	Time consuming	Sample amount required	Convenient	Cost	Purity, analytic, sensitivity	Automatic
Human	X	X	X	X	△	X
Tradition beads	△	△	△	X	X	△
Sample-preparation chip	O	O	O	O	O	O
O ： Better 、△ ：Common 、 X ：Bad						

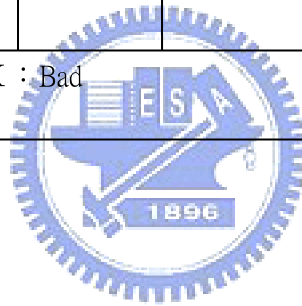

Chapter 5

Conclusions

We have successfully developed useful Cu diffusion barrier layer: The effects on the deposition rate, composition, crystal structure, and resistivity of TaN_X films as a function of their reactive gas source and gaseous flow ratio. As the flow ratio of the reactive gases increased, the structures of the TaN_X films changed from BCC－Ta to FCC－TaN to nanocrystalline－TaN. The growth of TaN_X films through RF sputtering using NH_3/Ar gas mixtures led to larger grain sizes and lower resistivities. The thermal stabilities of TaN_X films were dependent predominantly on their crystal structure, and less so on their gas source. Higher N/Ta ratios led to improved thermal stabilities of Cu/TaN_X/n^+np^+ diode structures, but the resistivity increased when the ratio was too high. At an N/Ta ratio of ca. 1, the films exhibited good thermal stability and moderate resistivity and behaved as high-performance Cu diffusion barriers.

We have also successfully developed roubast Cu CMP process: An IR thermal camera was used to choose a suitable non-Preston Cu CMP slurry and diagnose the Cu CMP process in real time. Additionally, using a robust CMP machine, a Cu film of appropriate quality, and a suitable pretreatment, enables the Cu CMP process to be greatly improved, with almost no Cu residues or defects.

We have also successfully integrated nano, bio and MEMS to develop a polymeric microfluidic biochip: The PMMA is chosen as the biochip substrate. The PMMA polymer solution is applied to treat the substrate surface to fix the DNA extraction beads, this approach provides an attractive intermolecular force between DNA and the substrate surface by the DNA extraction method base on results from PCR amplification and agarose gel electrophoresis testing. The brightness in the

agarose gel electrophoresis test indicates that as the electrophoresis diagrams have higher brightness, more DNA is attached in the test. A polymer solution can fix the DNA extraction beads on the substrate surface. In addition, plasma treatment on the substrate activates the surface and thus promotes covalent bonding of DNA extraction beads with the substrate surface and improves extraction efficiency. This study provides a practical and efficient method for LOC to be more realistic.

LIST OF PUBLICATIONS

(A) Journal

1. Yung-Chiang Chung, **Chia-Hao Chan**, Yu-Cheng Lin, Ju-Hwa Lin, Wang-Chin Cheng and Chia-Yu Fan ***"Microfluidic Chip for High Efficiency DNA Extraction"*** Lab Chip, **2004**, 141-147.

2. **Chia-Hao Chan**, Jem-Kun Chen and Feng-Chih Chang ***"In situ characterization of Cu CMP slurry and defect reduction using IR thermal camera"***Microelectronic Engineering, **2004**, 75, 257-262.

3. Jem-Kun Chen, I-Kuan Lin, Fu-Hsiang Ko, Chih-Feng Huang, Kuo-Shen Chen, **Chia-Hao Chan** and Feng-Chih Chang ***" Behavior and Surface Energy of Polybenzoxazines formed by Polymerization with Argon, Oxygen, and Hydrogen Plasmas"*** J. Polym. Sci., B: Polym. Phys., **2004**, 42, 4063-4074.

4. Jem-Kun Chen, Fu-Hsiang Ko, **Chia-Hao Chan**, Chih-Feng Huang and Feng-Chih Chang ***"Using imprinting technology to fabricate three-dimensional devices from moulds of thermosetting polymer patterns"*** Semicond. Sci. Technol., **2006**, 21, 1213–1220.

5. **Chia-Hao Chan**, Chih-Feng Huang, Jem Kun Chen and Feng-Chih Chang ***"Comparing nanoscale characterization of TaN_x barrier thin films prepared by NH_3/Ar and N_2/Ar reactive gases"*** Thin Solid Films, **2006**, submitted.

6. **Chia-Hao Chan**, Pei-Yi Ku, Chih-Feng Huang, Shiao-Wei Kuo, Jem Kun Chen and Feng-Chih Chang ***"Immobilization of DNA extraction beads in polymeric microfluidic biochip for sample-preparation"*** Sensors & Actuators: B. Chemical, **2006**, submitted.

(B) Conference

1. A. Shieh, J. Chen, Y.L. Hwang, S.Y. Shih, **Chia-Hao Chan** and J. X. Lin ***"Step-by-step characterization in the Cu-CMP by using Non-Preston slurry"*** CMP-MIC,**2001.**

(C) Patent

1. **Chan Chia-Hao** and Wang Chin-Horng ***"High-performance bio-tube for purifying DNA and method thereof"*** US patent, **2004,** 20040241656.
2. **Chan Chia-Hao** and Wang Chin-Horng *"高效能生醫試管及其去氧核糖核酸純化方法"* 中華民國專利, **2005,** 200500464.
3. Chung Yung-Chiang, **Chan Chia-Hao**, Lin Ju-Hwa and Huang Shr-Hau ***" Microfluidic mixer apparatus and microfluidic reactor apparatus for microfluidic processing"*** US patent, **2005,** 20050118647.

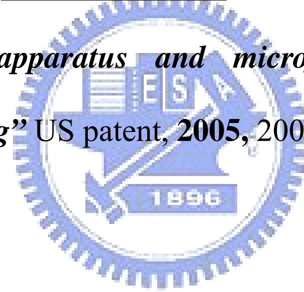

Introduction to the Author

English name: Chia-Hao Chan

Chinese name: 詹嘉豪

Birthday: 1975, 03, 20

Address: 310 新竹縣竹東鎮二重里自由街 120 巷 6 號 11 樓之 3

Education:

1993.09~1997.06	**B. S.,** Department of Chemical Engineering, Tunghai University, Taichung, Taiwan
1997.09~1999.06	**M. S.,** Institute of Chemical Engineering, National Taiwan University of Science and Technology University, Taipei, Taiwan
2002.09~2006.12	**Ph. D.,** Institute of Applied Chemistry, National Chiao Tung University, Hsin Chu, Taiwan